Algorithm Theoretical Basis Document

Atmospheric Corrections

Issued by: HYGEOS

Date: 29/03/2021

Ref: Proba-V-reprocessing-AC-ATBD_v1.01

Contract No : QA4EO CCN2 _XXXXX

Contributors

HYGEOS
Didier Ramon, Dominique Jolivet, Thierry Elias, Mathieu Compiègne

History of modifications

Version	Date	Description of modification	Chapters / Sections
V1.0	08/06/2020	Draft Initial version	All
V1.01	29/03/2021	Quality flag update	2.2.6
V1.02	03/03/2023	Editorial changes	

Acronyms

Acronym	Definition
6S	Second Simulation of the Satellite Signal in the Solar Spectrum
ADAS	Atmospheric Data Assimilation System
AERONET	Aerosol Robotic Network
AC	Atmospheric Correction
ACIX2	Atmospheric Corrections Intercomparison eXercise II
AOT	Aerosol Optical Thickness
ATBD	Algorithm Theoretical Basis Document
AVHRR	Advanced Very High Resolution Radiometer
B0, B2, B3	Spectral bands of the SPOT/VEGETATION sensor, in the blue, red and near infrared, respectively.
BC	Black Carbon aerosols
BRDF	Bi-directional Reflectance Distribution Function
BSA	Black-Sky Albedo
C3S	Copernicus Climate Change
CAMS	Copernicus Atmosphere Monitoring Service
DEM	Digital Elevation Model
DU	Dust aerosols
EOS	Earth Observation Satellites
FCDR	Fundamental Climate Data Record
GEOS	Goddard Earth Observing System
GPL	GNU Public Licence
GPU	Graphics Processing Unit
MERRA-2	Modern-Era Retrospective analysis for Research and Applications, Version 2
MISR	Multi-angle Imaging SpectroRadiometer (on board EOS)
MODIS	MODerate Imaging Spectrometer
NASA	National Aeronautics and Space Agency
NetCDF	Network Common Data Form
NIR	Near InfraRed
OC	Organic Carbon aerosols
RSRF	Relative Spectral Response Function
SAA	Sun Azimuth Angle
SMAC	Simplified Model for Atmospheric Corrections
SMAC-GPU	SMAC model implemented with GPU
SPOT	Satellite Probatoire d'Observation de la Terre
SRF	Spectral Response Function
SS	Sea Salt aerosols
SU	SUlphate aerosols

SWIR	Short-Wave InfraRed
SZA	Sun Zenith Angle
TOA	Top Of the Atmosphere
TOC	Top Of Canopy
TOC-r	Top Of Canopy Reflectance
TOMS	Total Ozone Mapping spectrometer
UTC	Universal Time Coordinates
VAA	View Azimuth Angle
VEGETATION	The medium resolution sensor onboard SPOT4 and SPOT5
VGT	VEGETATION sensor
VITO	Vlaamse Instelling voor Technologisch Onderzoek (Flemish Institute for Technological Research), Belgium
VZA	View Zenith Angle
WGS	World Geodetic System

Table of Contents

Scope of the document

This document describes the algorithm basis for performing Atmospheric Corrections for the PROBA-V Collection 2 surface reflectance data. It is applicable to all resolutions.

1. Input and auxiliary data

1.1 Input data

Band	Central wavelength (nm)	FWHM (nm)	Corrected	Absorbing gas/ transmission*
B1	463.5	47.0	yes	O_3 (0.994)
B2	655.0	80.0	yes	O_3 (0.976) ; H_2O (0.989) ; O_2 (0.981)
B3	839.0	130.0	yes	O_3 (0.999) ; H_2O (0.893) ; O_2 (0.999)
B4	1 602.5	65.0	yes	CO_2 (0.969); H_2O (0.995); CH_4 (0.998)

Table 1: PROBA-V spectral bands and potential atmospheric gaseous absorbers

The data used as input are Proba-V Top-Of-Atmosphere reflectances in 4 spectral bands (Table 1) and associated geometrical information and basic classification flags. Let us note that the viewing geometry is different between VIS-NIR and SWIR bands. The RSRF's of each band is slightly different between the 3 cameras labelled LEFT, CENTER and RIGHT that cover Proba-V field of view. The philosophy of the AC algorithm is to process the data band per band without the use of any spectral, spatial or temporal features. Therefore, the format of the input data is not important and the processing of individual pixels for selected bands or an entire Level 1 tile is similar.
The mandatory information is the following:

- `TOA-r`: TOA reflectance in bands `B1`, `B2`, `B3` and `B4` corrected from biases,
- `DTOA-r`: TOA reflectance in bands `B1`, `B2`, `B3` and `B4`,
- Latitude and longitude: `lat, lon`
- Status Map (`SM`), from which we use the Cloud mask,
- Viewing and solar azimuth angles (`VAA, VAA_SWIR` and `SAA`) [0, 360°]
- Viewing and solar zenith angles (`VZA, VZA_SWIR` and `SZA`) [0, 90°].

1.2 Auxiliary data

1.2.1 Digital Elevation Model

The GTOPO30 (Global 30 Arc-Second Elevation) dataset is used for assigning a surface elevation to each pixel. It is downloaded as a set of binary files (https://lta.cr.usgs.gov/GTOPO30) and then re-assembled as a unique NetCDF file.

- Frequency: Static
- Spatial Grid: 2D, full extent of latitude from 90 degrees south to 90 degrees north, and the full extent of longitude from 180 degrees west to 180 degrees east. The horizontal grid spacing is 30-arc seconds.
- Dimensions of 21,600 rows and 43,200 columns. The horizontal coordinate system is decimal degrees of latitude and longitude referenced to WGS84.

- The vertical units represent elevation above mean sea level (`elev`) and are expressed in meters. The values range from -407 to 8,752. It is complemented by the spatial standard deviation of the altitude (`Delev` in meters) computed in 3x3 pixel boxes.

1.2.2 Atmospheric Parameters

Two options are examined. Both relies on Atmospheric Global Reanalysis datasets which can be used easily for a reprocessing exercise. In both cases a derived climatology is going to be evaluated.

1.2.2.1 MERRA-2

The Modern-Era Retrospective analysis for Research and Applications version 2 (MERRA-2) is a NASA atmospheric reanalysis for the satellite era using the Goddard Earth Observing System Model, Version 5 (GEOS-5) with its Atmospheric Data Assimilation System (ADAS), version 5.12.4. It is the data source for all atmospheric parameters (https://gmao.gsfc.nasa.gov/reanalysis/MERRA-2/). The README file for the NetCDF MERRA-2 products is available here: (https://goldsmr4.gesdisc.eosdis.nasa.gov/data/MERRA2/M2I1NXINT.5.12.4/doc/MERRA2.README.pdf), while the full product specification is available here: (https://gmao.gsfc.nasa.gov/pubs/docs/Bosilovich785.pdf).

The datasets are available from 1st January 1980 until present. They can be downloaded from several sites, for example (https://disc.sci.gsfc.nasa.gov/daac-bin/FTPSubset2.pl).

Two products are currently used for all atmospheric parameters:

- `tavg1_2d_slv_Nx`: 2-dimensional, 1-Hourly, Time-Averaged for physical parameters, ozone and water vapour.
- `tavg1_2d_aer_Nx`: 2-dimensional, 1-Hourly, Time-Averaged for aerosol diagnostics.

Both of them have the same spatial and temporal grids:

- Frequency: 24 1-hourly from 00:30 UTC (time averaged)
- Spatial Grid: 2D, single-level, global Lat-Lon regular grid
- Lat: 361 values from -90 to 90
- Lon: 576 values from -180 to 179.375

1.2.2.2 Total Column Ozone

From `tavg1_2d_slv_Nx`. The parameter used is:
`TO3`: the total column ozone expressed in Dobson units.

1.2.2.3 Total Precipitable Water Vapor

`From tavg1_2d_slv_Nx`. The parameter used is:
`TQV`: the total precipitable water vapor expressed in kg.m^{-2}.

1.2.2.4 Sea-level Pressure

From `tavg1_2d_slv_Nx`. The parameter used is:
`SLP`: the sea-level pressure expressed in Pa.

1.2.2.5 Temperature above ground

From `tavg1_2d_slv_Nx`. The parameter used is:
`T10M`: the temperature above ground (10 m) in Kelvin.

1.2.2.6 Aerosol Optical Thicknesses

`From tavg1_2d_aer_Nx`. The parameters used are:
`TOTEXTTAU`: the total aerosol extinction optical thickness at 550 nm.
`BCEXTTAU`: the black carbon (BC) aerosol extinction optical thickness at 550 nm.
`OCEXTTAU`: the organic carbon (OC) aerosol extinction optical thickness at 550 nm.
`DUEXTTAU`: the dust (DU) aerosol extinction optical thickness at 550 nm.
`SUEXTTAU`: the sulfate (SU) aerosol extinction optical thickness at 550 nm.
`SSEXTTAU`: the sea salt (SS) aerosol extinction optical thickness at 550 nm.

1.2.3 EAC4 (ECMWF Atmospheric Composition Reanalysis 4)

This Global CAMS reanalysis (Innes et al. 2019) is the new European atmospheric composition reanalysis. Data and documentation are available through the Copernicus Climate Data Store.
https://ads.atmosphere.copernicus.eu/cdsapp#!/dataset/cams-global-reanalysis-eac4?tab=overview
It is a 3 hourly, 0.75x0.75° global gridded dataset, available since for the period 2003-2019. It is distributed either in GRIB or NetCDF formats.
One subsetted file can be ordered containing all the datasets needed for SMAC
Both of them have the same spatial and temporal grids:

- Frequency: 8 3-hourly from 00:00 UTC
- Spatial Grid: 2D, single-level, global Lat-Lon regular grid
- Lat: 241 values from -90 to 90
- Lon: 480 values from 0 to 359.25

1.2.3.1 Total Column Ozone

`gtco3`: the GEMS total column ozone expressed kg/m^2.

1.2.3.2 Total Column Water Vapor

`tcwv`: the total column water vapor expressed kg/m^2.

1.2.3.3 Sea-level Pressure

`msl`: Mean sea level pressure expressed in Pa.

1.2.3.4 Temperature above ground

`t2m` : 2 metre temperature expressed in Kelvin

1.2.3.5 Aerosol Optical Thicknesses

`aod550` : the total aerosol optical depth at 550nm
`bcaod550`: the black carbon (BC) aerosol optical depth at 550 nm.
`omaod550`: the organic carbon (OC) aerosol optical depth at 550 nm.
`duaod550`: the dust (DU) aerosol optical depth at 550 nm.
`suaod550`: the sulfate (SU) aerosol optical depth at 550 nm.
`ssaod550`: the sea salt (SS) aerosol optical depth at 550 nm.

1.2.4 SMAC Coefficients

These coefficients constitute the core of the SMAC algorithm. They have been calculated for Proba-V for the RIGHT, CENTER and LEFT cameras and for 148 aerosol models as described in the Appendix.

2. Algorithm

2.1 Computation of TOA reflectances and uncertainty

<u>Note</u>: In this section, among all the variables used in the AC algorithm, those that are constant (configuration parameters or inputs) are written in `Courier New` font (`input1`), those that are computed (intermediate variable or outputs) are written in Math font (Δx).

$$R_{toa}(\theta_s, \theta_v, \Delta\Phi) = \frac{\pi\, L(\theta_s, \theta_v, \Delta\Phi)}{\cos(\theta_s) E_s} \tag{1}$$

$$\Delta R_{toa}(\theta_s, \theta_v, \Delta\Phi) = \frac{\pi\, \Delta L(\theta_s, \theta_v, \Delta\Phi)}{\cos(\theta_s) E_s} \tag{2}$$

Where $L(\theta_s, \theta_v, \Delta\Phi)\ and\ \Delta L(\theta_s, \theta_v, \Delta\Phi)$ `TOA-r` and `DTOA-r` respectively, `Es` are is the extra-terrestrial solar irradiance and θ_s is `SZA` .

2.2 Atmospheric correction

2.2.1 Rationale

Pixels are considered for atmospheric correction if they are not marked as “cloud-covered” or “contaminated” in the cloud mask of input data. TOC directional reflectance estimates are obtained by applying SMAC (Rahman and Dedieu, 1994), a Simplified Method for the Atmospheric Correction of satellite measurements in the solar spectrum to the TOA reflectances.

The choice of the SMAC algorithm is supported by the following arguments:

- It is operational and largely used in the land community and already implemented in the Copernicus Global Land Service processing lines.
- It is a robust and generic algorithm, thus it minimizes the dependence on the sensor which is a good thing when one wants to build a multi sensor long time series with limited biases.
- The formulation of the algorithm is analytical and is adapted to an error propagation analysis.

2.2.2 Overview

SMAC is based on the 6S radiative transfer formulation of the satellite signal (Vermote et al., 1997) where all the pertinent radiative quantities are parameterized as a function of auxiliary data:

- Gas content (mainly ozone and water vapor for the spectral channels considered in this project)
- Aerosol content and aerosol type
- Molecular scattering mainly driven by the sea-level surface pressure and the surface elevation.

The atmospheric correction is performed for <u>each band separately</u> and the basic equations of SMAC are:

$$T = T_g(\theta_s, \theta_v)\ T_{sca}(\theta_s)\, T_{sca}(\theta_v) \tag{3}$$

$$R = R_{toa} - R_{atm}(\theta_s, \theta_v, \Delta\Phi)\ T_g(\theta_s, \theta_v) \tag{4}$$

$$R_{toc}(\theta_s, \theta_v, \Delta\Phi) = \frac{R}{T + s_{atm} R} \tag{5}$$

where the inputs are the geometry ($\mathrm{SZA}\ \theta_s$, $\mathrm{VZA}\ \theta_v$, and $\mathrm{RAA}\ \Delta\Phi$), the pixel geolocation, the TOA reflectances R_{toa} and the outputs are the TOC directional reflectances R_{toc}. The auxiliary data are used to compute the total gaseous transmission T_g, the atmospheric path radiance R_{atm}, the atmospheric spherical albedo s_{atm} and the total downward and upward scattering transmissions T_{sca}. These computations are done for each sensor's channel according to the SMAC parameterization and for one aerosol model. From Eq. (3) to (5), it is possible to derive the atmospherically corrected TOC directional reflectance uncertainty ΔR_{toc} from the uncertainties on the TOA reflectance and on the atmospheric reflectances and transmittances, which are themselves derived from the uncertainties on the gaseous content, surface pressure aerosol load and type.

2.2.3 Error propagation

2.2.3.1 TOA reflectance uncertainty

The radiometric uncertainty of the TOA reflectance is ΔR_{toa}. The resulting uncertainty on the TOC directional reflectance $\Delta_{R_{toc}}^{R_{toa}}$, is obtained:

$$\Delta_{R_{toc}}^{R_{toa}} = \left| \frac{\partial R_{toc}}{\partial R_{toa}} . \Delta R_{toa} \right| \tag{6}$$

where $\frac{\partial R_{toc}}{\partial R_{toa}}$ is the sensitivity of TOC directional reflectance to any change in TOA reflectance. It is the Jacobian $J_{R_{toc}}^{R_{toa}}$.

Within SMAC, it can be derived analytically:

$$J_{R_{toc}}^{R_{toa}} = \frac{\partial R_{toc}}{\partial R} \frac{\partial R}{\partial R_{toa}} \tag{7}$$

after remarking that $\frac{\partial R}{\partial R_{toa}} = 1$, and using Eqs. (4) and (5)

$$\eta = 1/(T + s_{atm} R) \tag{8}$$

$$J_{R_{toc}}^{R_{toa}} = \eta^2\ \mathrm{T} \tag{9}$$

2.2.3.2 Auxiliary data uncertainty

2.2.3.2.1 Ozone and Water Vapor

The sensitivity of TOC directional reflectance to the uncertainty in the total column of either ozone or water vapor is also treated analytically within SMAC. In the following, we apply the equation for the gas X, with X being O_3 or H_2O.

The uncertainty in the total column U_X is propagated through the Jacobian $J_{R_{toc}}^{U_X}$.

$$\Delta_{R_{toc}}^{U_X} = \left| J_{R_{toc}}^{U_X} . \Delta U_X \right| \tag{10}$$

Within SMAC, it can also be derived analytically.

Let us recall the formulation of the transmission of the gas T_X:

$$T_X = e^{\,a_X (U_X m)^{n_X}} \tag{11}$$

where a_X and n_X are SMAC coefficients and m is the air mass:

$$m = \frac{1}{\cos \theta_s} + \frac{1}{\cos \theta_v} \tag{12}$$

We decompose the Jacobian into two parts:

$$J_{R_{toc}}^{U_X} = \frac{\partial R_{toc}}{\partial T_X} . \frac{\partial T_X}{\partial U_X} \tag{13}$$

The sensitivity of T_X to U_X is:

$$\frac{\partial T_X}{\partial U_X} = \left(\frac{a_X . n_X}{U_X} \right) . \ (U_X m)^{n_X} . T_X \tag{14}$$

The sensitivity of TOC directional reflectance to T_X is obtained through Eq. (3), (4) and (5) and using the decomposition $T_g = T_X \,. T_{noX}$:

$$\frac{\partial R_{toc}}{\partial T_X} = -\eta^2 \frac{T R_{toa}}{T_X} \tag{15}$$

2.2.3.2.2 Surface Pressure and AOT at 550 nm

For the surface pressure P_s and the AOT at 550 nm τ_a^{550}, we process the pixel two times more with small perturbations δP_s and $\delta \tau_a^{550}$, and then derive the Jacobians using the finite differences:

$$J_{R_{toc}}^{P_s} = \frac{\mathrm{R}_{toc}(P_s) - \rho_{toc}(P_s - \delta P_s)}{\delta P_s}, \tag{16}$$

$$\Delta_{R_{toc}}^{P_s} = \left| J_{R_{toc}}^{P_s} . \Delta P_s \right|, \tag{17}$$

$$J_{R_{toc}}^{\tau_a^{550}} = \frac{R_{toc}(\tau_a^{550}) - R_{toc}(\tau_a^{550} - \delta \tau_a^{550})}{\delta \tau_a^{550}} \tag{18}$$

$$\Delta_{R_{toc}}^{\tau_a^{550}} = \left| J_{R_{toc}}^{\tau_a^{550}} . \Delta \tau_a^{550} \right| \tag{19}$$

We use $\delta P_s = 10\ hPa, \delta\tau_a^{550} = 0.1\ \tau_a^{550}$. These values are chosen for provoking a sufficient response in the AC scheme and still staying in the linear regime.

2.2.3.3 Combination

The individual errors are supposed independent and Gaussian. They are combined quadratically:

$$\Delta R_{toc} = \sqrt{\left[\left(\Delta_{R_{toc}}^{R_{toa}}\right)^2 + \left(\Delta_{R_{toc}}^{U_{H_2O}}\right)^2 + \left(\Delta_{R_{toc}}^{U_{O_3}}\right)^2 + \left(\Delta_{R_{toc}}^{P_s}\right)^2 + \left(\Delta_{R_{toc}}^{\tau_a^{550}}\right)^2\right]} \tag{20}$$

2.2.3.4 Limitations

The SMAC algorithm is a parameterization of the radiative transfer model 6S (Vermote et al., 1997). 6S commonly agreed accuracy is 1%. SMAC approximation to 6S is also claimed to be within 1% for most situations under the assumption of lambertian surface (e.g. isotropic). For anisotropic surfaces however, the SMAC approximation could be quite inaccurate to several %, especially for high atmospheric turbidity. Neither adjacency effects nor terrain slope correction is applied in this project. These effects are however secondary at the spatial scale of 1 km or lower.

Approximations in radiative transfer lead essentially to biases, depending on surface, angles and atmospheric content, and are certainly not a source of random noise. This source of error is thus not yet included in the error propagation model, but we have the tools to estimate it at least statistically (see Appendix).

2.2.4 Errors characterization

2.2.4.1 TOA reflectance

The error on TOA radiance ΔL_{toa}comes from the inputs. As they are not yet validated, there is the option to ignore them.

2.2.4.2 Ozone and Water Vapor

The error characterization of atmospheric auxiliary data is mainly based on available publications of the MERRA-2 teams. A recent (2017) MERRA-2 dedicated issue of *Journal of Climate* is available here (http://journals.ametsoc.org/topic/merra-2)

For ozone, according to the last reference (Wargan et al., 2017, Davis et al., 2017*), the* MERRA-2 total column ozone agrees with TOMS data (1980-1993) very well, with less than 2 % bias and less than 6 % difference standard deviation, close to the assumed observation error of 5 %.

Davis et al., (2017) also analyzed the performances of re-analyses for water vapor, but not for the Total Column Water Vapor. We arbitrary fixed the uncertainty on total precipitable water vapor (TQV) to 20%, but this should be further investigated in the validation phase.

2.2.4.3 AOT at 550 nm

Randles et al. (2017) and Buchard et al., (2017) have evaluated the accuracy of the aerosols parameters within MERRA-2. The first one focuses on the aerosol assimilation description and verification by comparing AOT at 550 nm to the hourly averaged AERONET AOT. The latter performs comparisons to independent data sets such as Aerosol Absorption OT, vertical profiles and stratospheric AOT, ground based $PM_{2.5}$ measurements (Particulate Matter with diameter lesser than 2.5µm). Let us recall that MERRA-2 is assimilating the following aerosols data: AVHRR radiances over ocean, transformed empirically into equivalent AOD, before EOS era (1980-1999), and then MISR AOT over bright surfaces, MODIS AOD retrieval above dark targets and land based AERONET level 2 AOD since 1997.

In Figure 1 is plotted the regressions of AOT at 550 nm for 1998 and 2012. We give also the logarithm regressions in Figure 2 in order to compare with Randles et al., (2017) analysis.
The performance of the MERRA-2 aerosols description is far better for the 1999-present era than for the 1980-1999. We confirm the Randles et al. numbers, a global RMS error of the log of AOT of 0.48 in 2012 and 0.77 in 1998. It translates in a RMS error of 0.13 for τ_a^{550} in 2012 and 0.21 in 1998.
We added also in the AOT regression plots the quantity gfrac, defined as the proportion of match-ups that are satisfying the criteria following the metric recommended by Breon et al., (2011).

$$|\,\tau_a^{550}(MERRA2) - \tau_a^{550}(Aeronet)| < 0.05 + 0.15\tau_a^{550} \qquad (21)$$

A high *gfrac* (like 0.83 for 2012) reflects the fact that the uncertainty of the MERRA-2 AOT is within the experimental error of the assimilated AOT data that come from EOS sensors. For the pre EOS era, like in 1998, the regressions are poorer and *gfrac* is only 0.63. A *gfrac* value of 0.8 for pre EOS is obtained if we characterize the typical uncertainty of MERRA-2 AOT as $0.07 + 0.20\tau_a^{550}$

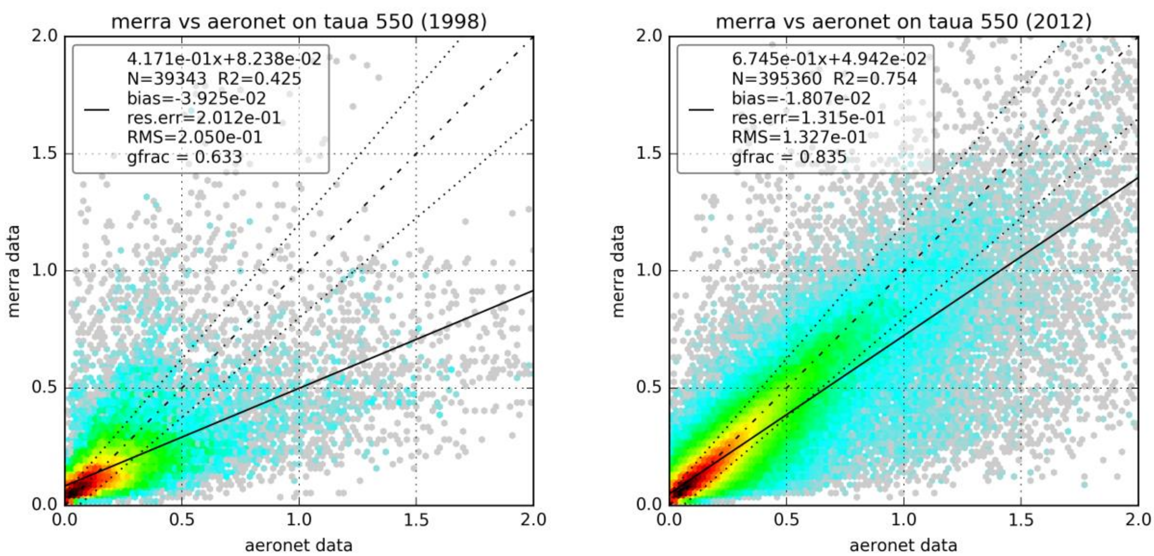

Figure 1: Example on AERONET/MERRA2 correlation plot for AOT at 550nm for all available AERONET stations and two representative years (before and after EOS launch). AERONET level 1.5 data are hourly averaged.

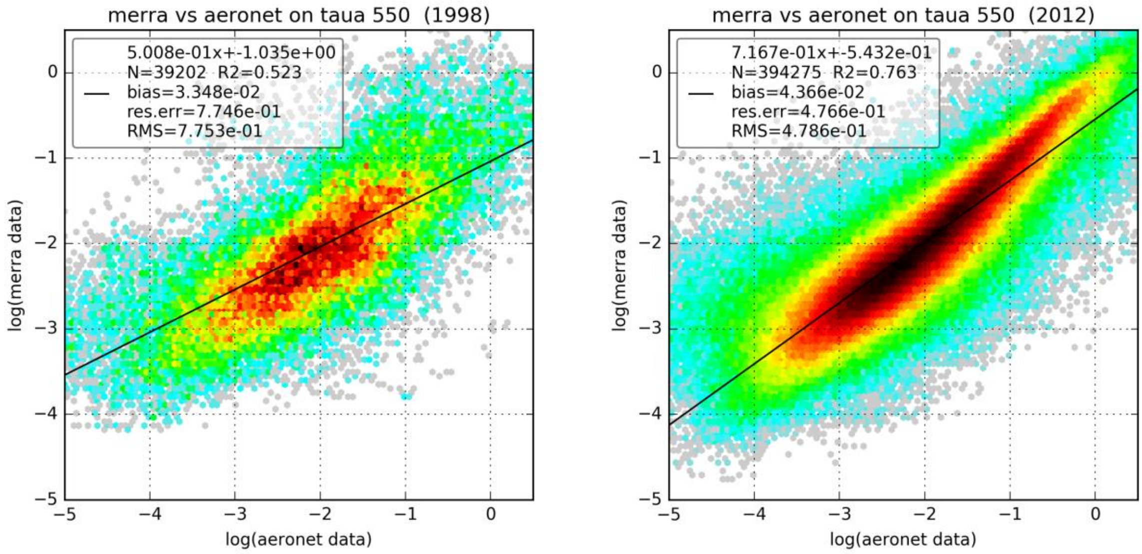

Figure 2: Same as Figure 1 but for the natural logarithm of AOT

2.2.4.4 Surface Pressure

The uncertainty on the surface pressure P_S is due to the uncertainty on the meteorological sea level pressure P_0 from MERRA-2 `SLP` parameter (very low, <1 hPa), and the way the extrapolation to the altitude of the surface z is done. z is obtained through GTOPO30 `elev`, which has a resolution close to the targeted satellite product. The uncertainty in the mean altitude of the pixel is Δz.

The surface pressure P_s is derived as:

$$\mathrm{P_S} = \mathrm{P_0}\ e^{-\frac{g}{r\lambda}T'} \tag{22}$$

$$T' = \ln(rT) - \ln(rT - r\lambda z) \tag{23}$$

Where T is the temperature above ground (from MERRA-2 `T10M` parameter), g is Earth's gravity (9.80665 m.s^{-2}), r is the gas constant for dry air (287.058 J.kg^{-1}.K^{-1}) and λ is the lapse rate *of the atmosphere, here taken* as −0.006 K.m^{-1} (*Van Besselaar et al., 2011*). The accuracy of this model depends on the variability of λ (typically $\Delta\lambda = 0.002$ K.m^{-1}). An uncertainty of $\Delta^{\lambda}_{P_s}$~1hPa could be assigned to this modeling error.

However, the uncertainty in the geolocation could result in a significant uncertainty Δz, especially in rough terrain. The latter error could be partly a random error and a pixel dependent bias.
For example, if the geolocation error is purely random and isotropic, with a stable standard deviation, one may pre-calculate the standard deviation of the surface altitude as shown in Figure 3.

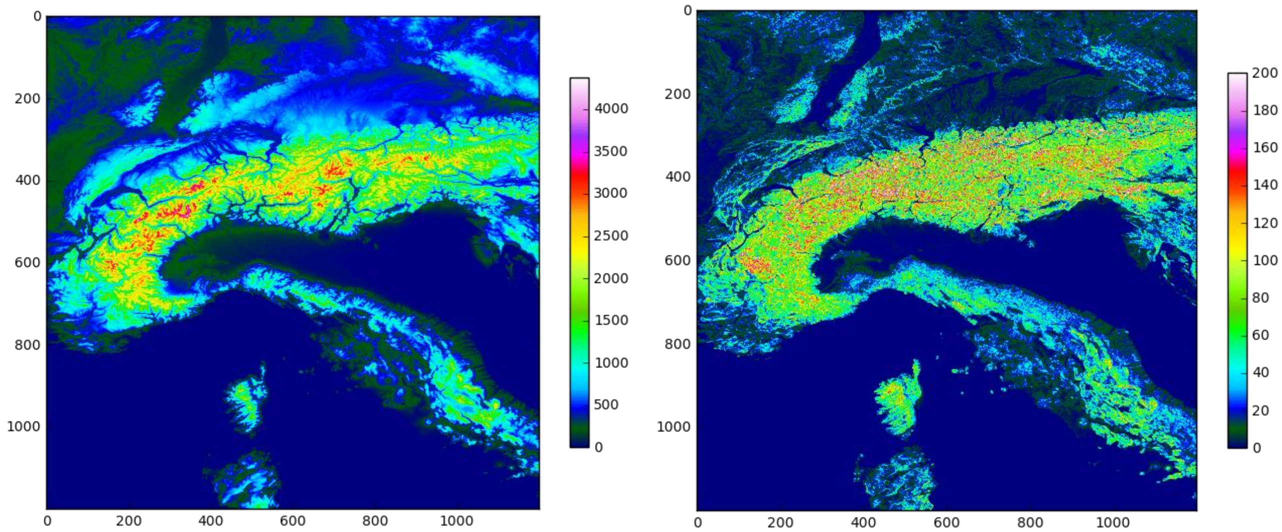

Figure 3: Surface elevation (left) and local standard deviation of altitude (right), both in m, from GTOPO30.

We implemented the computation of the local standard deviation of the surface altitude as an experimental auxiliary dataset within the DEM NetCDF file. The dataset named `Delev` has been computed from the convolution of `elev` with a gaussian averaging kernel with a parameter σ = 0.5 (in GTOPO30 bin unit, e.g 30 arc second). This correpsonds to the geometric accuracy of SPOT/VGT (0.3 pixel)

Finally, the uncertainty on P_s is:

$$\Delta P_s = \sqrt{\left[\left(\Delta_{P_s}^{\lambda}\right)^2 + \left(\Delta_{P_s}^{z}\right)^2\right]/2} \tag{24}$$

with

$$\Delta_{P_s}^{z} = \left|J_{P_s}^{z}.\Delta z\right| \tag{25}$$

and

$$J_{P_s}^{z} = -\frac{gP_S}{r(T-\lambda z)} \tag{26}$$

2.2.4.5 Summary

We summarize in Table 2 the individual errors applied in the first version of the AC.

Table 2: Summary of input uncertainty estimates

Uncertainty	*Source*	*Value*	*Note*
ΔR_{toa}	From FCDR Level 1/pixel	%	
ΔU_{O_3}	Auxiliary data/statistical	6%	See Wargan et al., (2017), Davis et al., (2017)

ΔU_{H_2O}	Auxiliary data/statistical	20%	
$\Delta P_0,\ \Delta\lambda$	Auxiliary data/statistical	<1 hPa , 0.002 K.m^{-1}	See van den Besselaar et al., (2011)
Δgeo	From Level 1/ pixel	<0.3 pixel	Proba-V geometrical accuracy
Δz	From FCDR Level 1 and auxiliary data/pixel	= f (DEM, Δgeo) OR Auxiliary `Delev` parameter	Complex on the fly computation OR If 2D geolocation error is considered random and its std. dev. is fixed, it can be stored in LUT with the DEM (convolution).
ΔP_S	From FCDR Level 1 and auxiliary data/pixel	From ΔP_0, $\Delta\lambda$: $\Delta_{P_S}^{\lambda}$~1hPa and from Δz using Eq. (25) and (26)	depending on altitude and temperature vertical profile, See van den Besselaar et al., (2011)
$\Delta\tau_a^{550}$	Auxiliary data/statistical	0.05 + 0.15τ_a^{550} (2000-present) 0.07 + 0.20 τ_a^{550} (1980-1999)	See Randles et al., (2017), and section 2.2.4.3.

2.2.5 Implementation

The SMAC algorithm has been implemented in C and Python under the GPL license (see for example http://www.cesbio.ups-tlse.fr/fr/modeles/modeles_list_8.html). We have decided to move to parallel based processing because it is a mature technology now, and we intend to run the SMAC algorithm a large number of times for each pixel in the forthcoming versions of the AC procedure. For this purpose, a new version called SMAC-GPU has been developed with the OPEN-CL graphics card programming language that includes the error propagation model with a Python interface. Details are given in Appendix.

2.2.6 Quality Flag

After the atmospheric corrections a bad radiometric flag is raised in the TOC-r Status Map dataset if one of the following condition is met:

TOC-r < TOCMIN in one or more of the 4 bands
TOC-r > TOCMAX in one or more of the 4 bands
SZA > SZAMAX

The choice for the TOC-r and SZA thresholds are coming from C1 heritage. For AOTMAX it relies on C3S experience. The thresholds are stored in the configuration file. They are currently set to

TOCMIN	0.0000

TOCMAX	1.0235
SZAMAX	80.0

3. Validation

3.1 Methodology

TOC-r's obtained with several aerosol ancillary data are validated with in-situ reference product obtained from AERONET data (version 3 of inverted AOD, spectral index of refraction and volume particle size distribution) and the 6S accurate atmospheric correction method. The comparison is performed for N=48 AERONET sites (see Figure 4) that cover different biomes, locations and meteorological conditions. Extraction of Proba-V data TOA-r and TOC-r' is done for 300 m products and TOA-r are processed with the 6S atmospheric correction software with AERONET data as inputs as it is done in the ACIX project (see **Error! Reference source not found.**). TOC-r are evaluated using t he same metrics as in ACIX

$$A = \frac{1}{N}\left(\sum_{i=1}^{N} \Delta toc\_r_i \right), \quad \text{Accuracy}$$

$$P = \sqrt{\frac{1}{N-1}\left(\sum_{i=1}^{N}\left(\Delta toc\_r_i - A\right)^2\right)}, \quad \text{Precision}$$

$$U = \sqrt{\frac{1}{N}\sum_{i=1}^{N}\left(\Delta toc\_r_i\right)^2}, \quad \text{Uncertainty}$$

with $\Delta toc\_r_i = \left(toc\_r_i^{processor} - toc\_r_i^{Aeronet}\right)$,

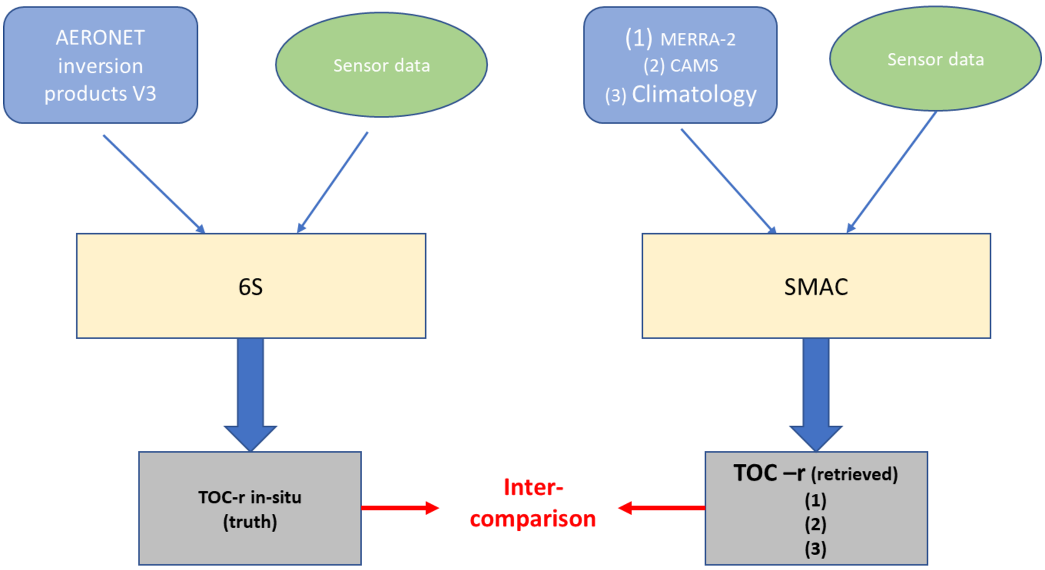

Figure 4 : Validation methodology logic

Site	Latitude	Longitude	Country	Site	Latitude	Longitude	Country
Anmyon	36.53	126.33	South Korea	La_Parguera	17.97	-67.04	Puerto Rico
Arica	-18.47	70.31	Chile	Lille	50.61	3.14	France
Banizoumbou	13.54	2.66	Niger	Mexico_City	19.33	-99.18	Mexico
Barrow	71.31	-156.66	Alaska (US)	Minsk	53.92	27.6	Belarus
Beijing	39.97	116.38	China	Mongu_Inn	-15.26	23.13	Zambia
Bonanza_Creek	64.74	-148.31	Alaska (US)	Moscow_MSU_MO	55.7	37.52	Russia
Bondville	40.05	-88.37	Illinois (US)	Palaiseau	48.71	2.21	France
Capo_Verde	16.73	-22.93	Sal Island (Capo Verde)	Rimrock	46.48	-116.99	Idaho (US)
Carpentras	44.08	5.05	France	Rio_Branco	-9.95	-67.86	Brazil
Cartel	45.37	-71.93	Canada	Rome_Tor_Vergata	41.83	12.64	Italy
Cart_Site	36.6	-97.48	Oklahoma (US)	Sao_Paulo	-23.56	-46.73	Brazil
Ceilap-BA	-34.55	-58.5	Argentina	Saturn_Island	48.77	-123.12	Canada
Cuiaba-Miranda	-15.73	-56.07	Brasil	Sede_Boker	30.85	34.78	Israel
Dakar	14.39	-16.95	Senegal	Sevilleta	34.35	-106.88	New Mexico (US)
Dhaka_University	23.72	90.39	Bangladesh	Shirahama	33.69	135.35	Japan
Dalanzadgad	43.57	104.41	Mongolia	Sioux_Falls	43.73	-96.62	South Dakota (US)
Egbert	44.23	-79.78	Canada	Skukuza	-24.99	31.58	South Africa
El_Arenosillo	37.1	-6.73	Spain	Tamanrasset_INM	22.79	5.53	Algeria
Forth_Crete	35.33	25.28	Greece	Thompson_Farm	43.1	-70.94	New Hampshire (US)
GSFC	38.99	-76.83	Maryland (US)	Tomsk	56.47	85.04	Russia
Ilorin	8.48	4.67	Nigeria	Toravere	58.26	26.46	Estonia
IMS-METU-Erdemli	36.56	34.25	Turkey	Venise	45.31	12.5	Italy
Jabiru	-12.66	132.89	Australia	Wallops	37.93	-75.47	Virginia (US)
Kanpur	26.51	80.23	India				

Table 3: List of Aeronet sites used for validation

3.1 Preliminary results

A first validation exercise has been done for the year 2018 and for the single Proba-V pixel closest to the Aeronet site. MERRA-2 hourly data was used as ancillary data. Regressions are plotted for all sites on Figure 5 and APU's are reported in Figure 6. Per pixels TOC-r uncertainties are not yet validated. No major flaws are detected but the validation should continue with others ancillary data and looking at potential causes of the biases.

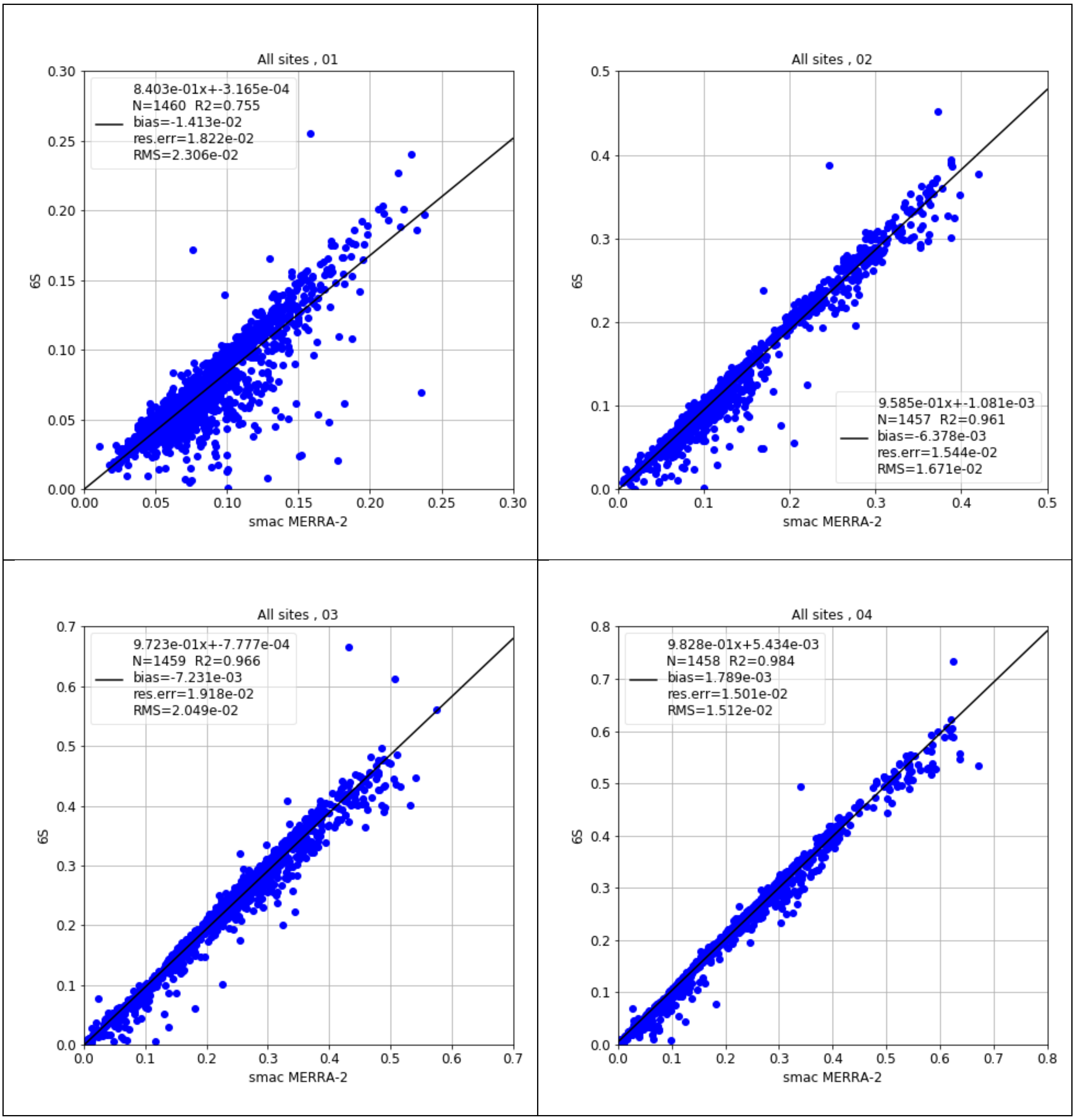

Figure 5: Regression of TOC-r for in the 4 Proba-V bands processed with SMAC-MERRA2 and TOC-r processed with 6S-AERONET for all sites in 2018.

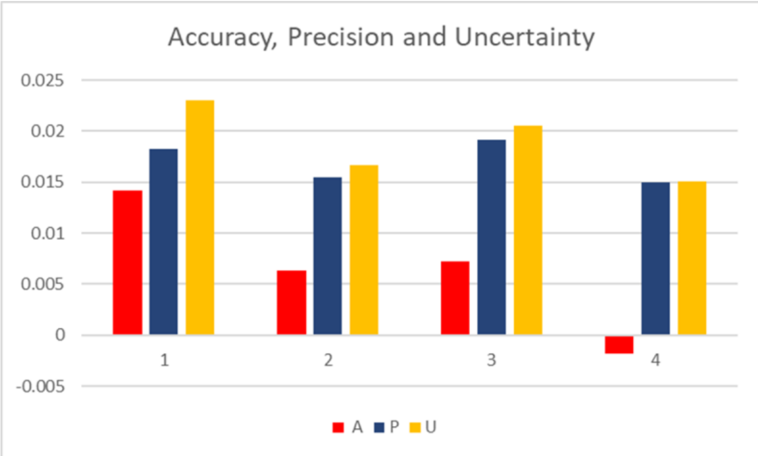

Figure 6: APU metrics corresponding to Figure 5

References

Breon, F.-M., A. Vermeulen and J. Descloitres, An evaluation of satellite aerosol products against sunphotometer measurements, *Remote Sensing of Environmen*t, Volume **115**, Issue 12, pp 3102-3111, 2011. https://doi.org/10.1016/j.rse.2011.06.017.

Buchard, V., C.A. Randles, A.M. da Silva, A. Darmenov, P.R. Colarco, R. Govindaraju, R. Ferrare, J. Hair, A.J. Beyersdorf, L.D. Ziemba, and H. Yu, The MERRA-2 Aerosol Reanalysis, 1980 Onward. Part II: Evaluation and Case Studies. *J. Climate*, **30**, 6851–6872, 2017. https://doi.org/10.1175/JCLI-D-16-0613.1

Davis, S. M., Hegglin, M. I., Fujiwara, M., Dragani, R., Harada, Y., Kobayashi, C., Long, C., Manney, G. L., Nash, E. R., Potter, G. L., Tegtmeier, S., Wang, T., Wargan, K., and Wright, J. S., Assessment of upper tropospheric and stratospheric water vapor and ozone in reanalyses as part of S-RIP*, Atmos. Chem. Phys.*, **17**, 12743-12778, 2017.

Inness, A., Ades, M., Agustí-Panareda, A., Barré, J., Benedictow, A., Blechschmidt, A.-M., Dominguez, J. J., Engelen, R., Eskes, H., Flemming, J., Huijnen, V., Jones, L., Kipling, Z., Massart, S., Parrington, M., Peuch, V.-H., Razinger, M., Remy, S., Schulz, M., and Suttie, M.: The CAMS reanalysis of atmospheric composition, *Atmos. Chem. Phys.*, **19**, 3515–3556, https://doi.org/10.5194/acp-19-3515-2019, 2019.

Rahman H. and G. Dedieu, SMAC: a simplified method for the atmospheric correction of satellite measurements in the solar spectrum. *Intern. J. Remote Sens*., **15**, 123-143, 1994.

Randles, C.A., A. M. da Silva, V. Buchard, P. R. Colarco, A. Darmenov, R. Govindaraju, A. Smirnov, B. Holben, R. Ferrare, J. Hair, Y. Shinozuka, and C. J. Flynn, The MERRA-2 Aerosol Reanalysis, 1980 Onward. Part I: System Description and Data Assimilation Evaluation. *Journal of Climate* **30**:17, 6823-6850, 2017.

Vermote, E.F., D. Tanré, J.L. Deuzé, M. Herman and J.-J. Morcrette, Second Simulation of the Satellite Signal in the Solar Spectrum, 6S: An Overview, *IEEE Transactions on Geoscience and Remote Sensing,* Vol. **35**, No. 3, p. 675-686, 1997.

van den Besselaar, E. J. M., M. R. Haylock, G. van der Schrier, and A. M. G. Klein Tank, A European daily high-resolution observational gridded data set of sea level pressure, *J. Geophys. Res.*, **116**, D11110, 2011. doi:10.1029/2010JD015468.

Wargan, K., G. Labow, S. Frith, S. Pawson, N. Livesey, and G. Partyka, Evaluation of the Ozone FIELDS in NASA's MERRA-2 Reanalysis, *J. Climate*, **16**, 2017, doi:10.1175/JCLI-D-16-0699.1.

4. Appendix

4.1 Appendix 1: Spectral response functions and gaseous absorption

We give here typical atmospheric gaseous transmissions in the Proba-V spectral bands and the RSRF for the CENTER camera. All radiative transfer computations have also been done for LEFT and RIGHT cameras RSRF's

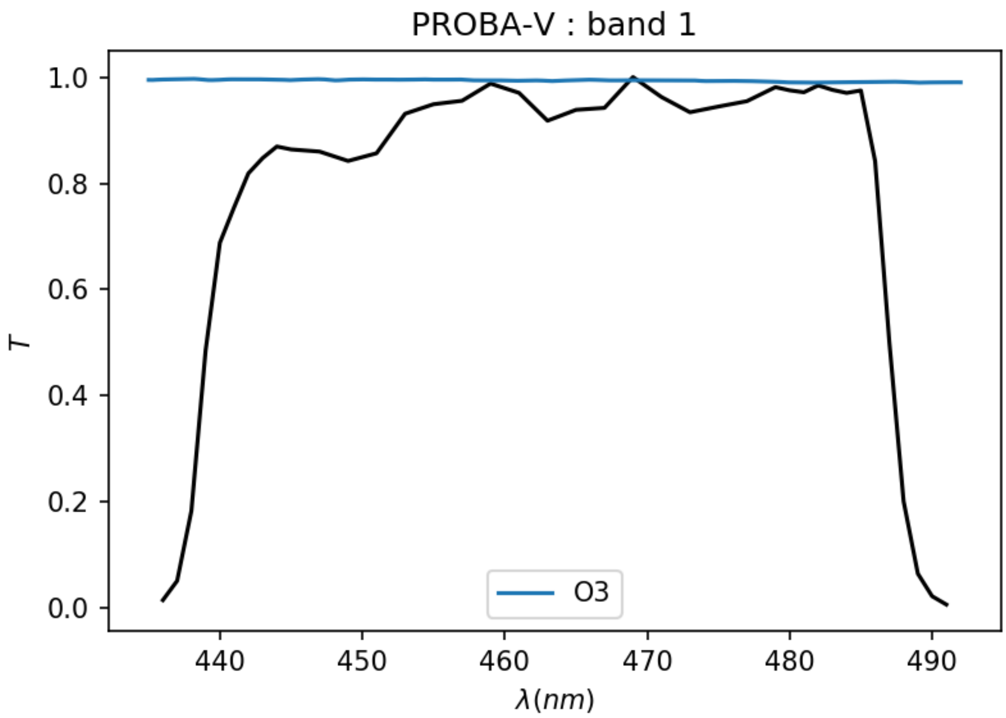

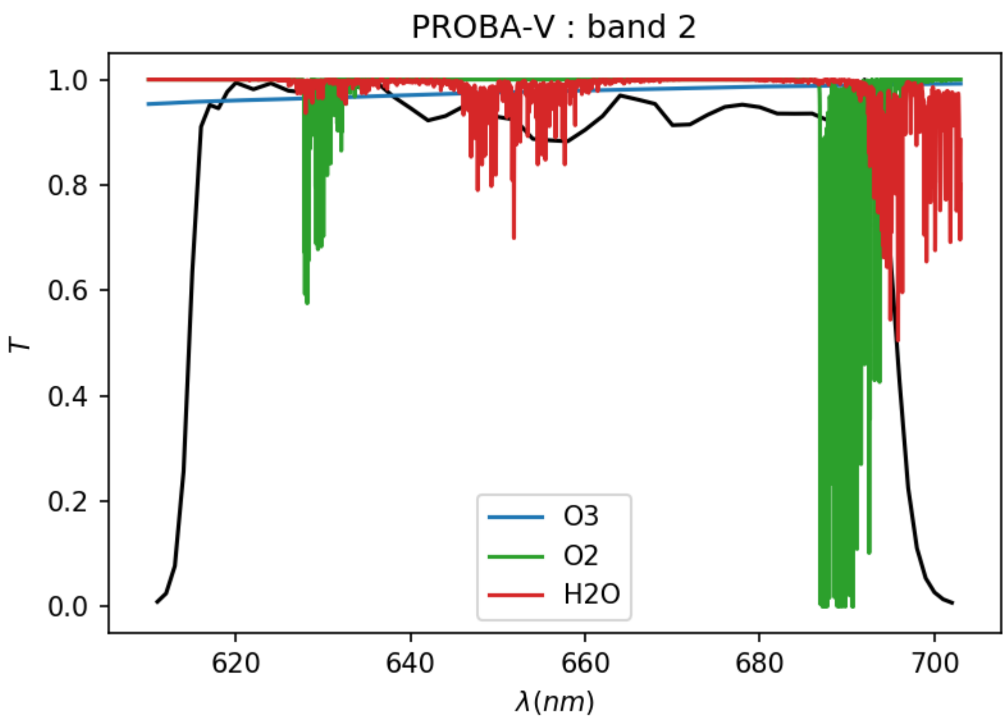

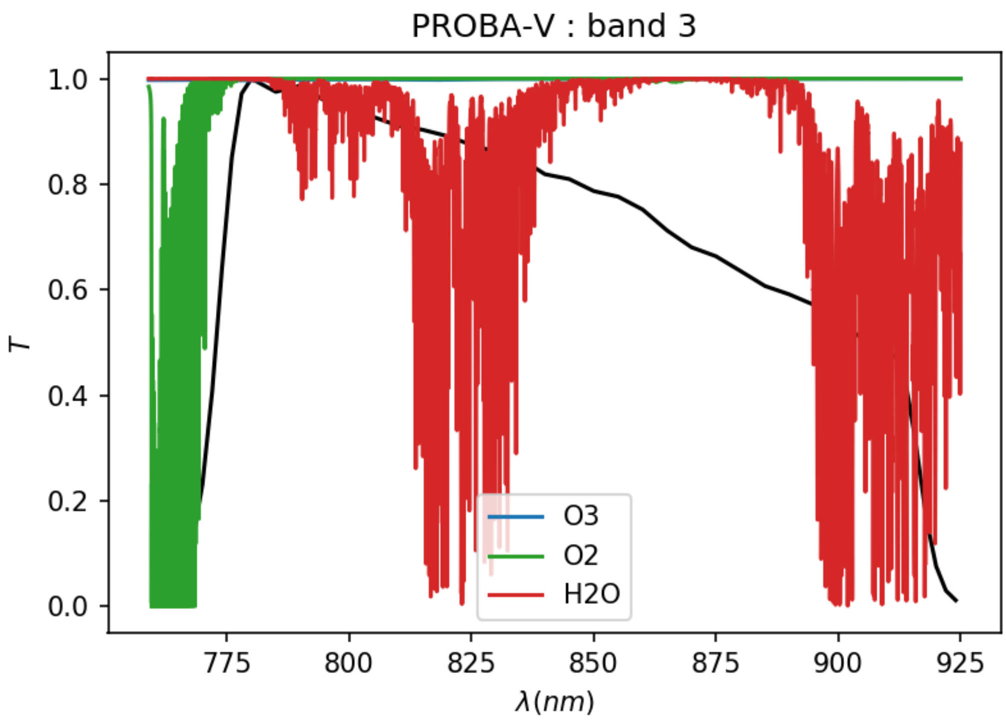

PROBA-V : band 3
1.0
0.8
0.6
0.4
0.2
0.0
T
775
800
825
850
875
900
925
λ(nm)
O3
O2
H2O

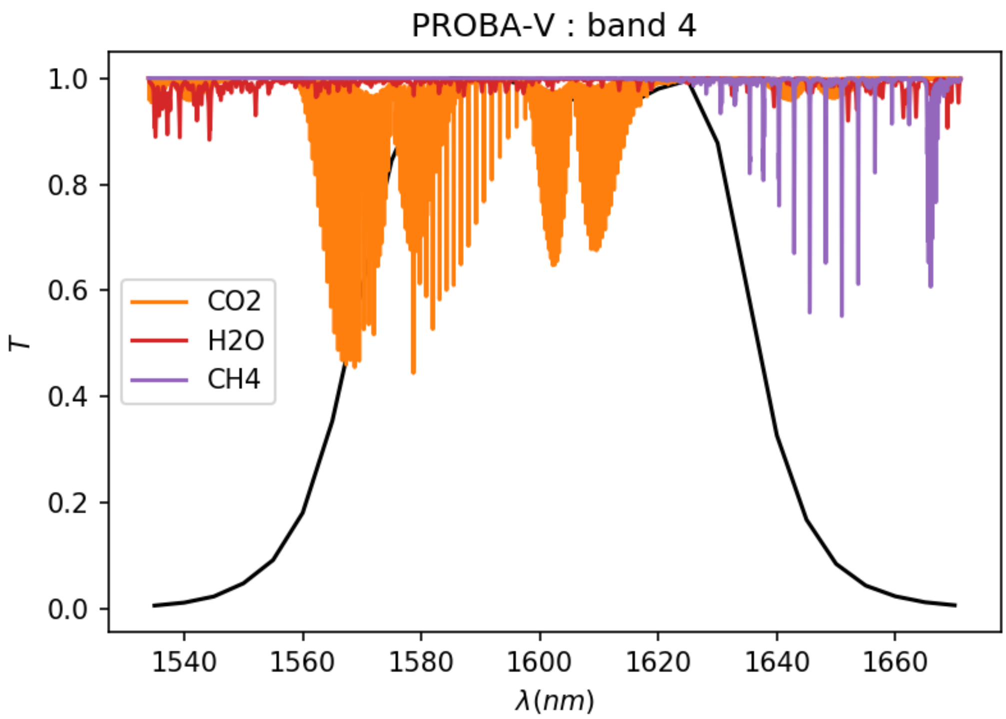

PROBA-V : band 4
1.0
0.8
0.6
0.4
0.2
0.0
T
1540
1560
1580
1600
1620
1640
1660
λ(nm)
CO2
H2O
CH4

4.2 Appendix 2: Aerosol models

4.2.1 Aerosol variability on Earth

44 688 MERRA-2 grid points have been selected over land. Four dates have been chosen to represent the seasonal variability: 2011/01/01, 2011/04/01, 2011/07/01, and 2011/10/01. Data are taken at 13:00.

Global average of AOT is computed for each component for the four dates. The total AOT increases from winter to summer, especially because of desert dust and OC. Indeed desert dust AOT increases from 0.04 to 0.10 and OC AOT from 0.02 to 0.05. The three other component AOT vary little with the season.

The aerosol models are defined according to the MERRA-2 or CAMS 5 AOT ratios of each aerosol component u {X_u, u ∈ $\{\mathrm{DU}, \mathrm{SU}, \mathrm{OC}, \mathrm{BC}, \mathrm{SS}\}$}:

$X_u = \boldsymbol{\tau_{a;u}^{550}} / \boldsymbol{\tau_a^{550}}$

1 Jan. 2011		Xu (%)				
u	AOT	min - max	P_{10},P_{50},P_{90}	mean	range	step
SU	0.06±0.09	2-94	17, 39, 66	49±20	0-100	20
DU	0.04±0.10	0-93	3, 13, 61	22±23	0-100	20
OC	0.02±0.04	0-63	6, 12, 29	15±10	0-70	20
SS	0.01±0.02	0-89	1, 3, 25	9±13	0-100	20
BC	<0.01	0-25	2, 5, 9	5±3	0-30	5
Total	0.14					
1 Apr. 2011		Xu (%)				
u	AOT	min - max	P_{10},P_{50},P_{90}	mean	range	step
SU	0.08±0.13	1-96	12, 42, 65	40±20	0-100	20
DU	0.09±0.17	0-97	6, 23, 74	31±25	0-100	20
OC	0.03±0.04	1-74	6, 16, 33	18±11	0-100	20
SS	0.01±0.02	0-88	1, 2, 17	6±11	0-100	20
BC	<0.01	0-17	2, 5, 8	5±2	0-30	5
Total	0.22					
1 Jul. 2011		Xu (%)				
u	AOT	min - max	P_{10},P_{50},P_{90}	mean	range	step
SU	0.07±0.12	1-98	12, 30, 55	32±16	0-100	20
DU	0.10±0.20	0-98	6, 18, 71	29±24	0-100	20
OC	0.05±0.07	0-87	5, 21, 54	26±19	0-100	20
SS	0.01±0.03	0-89	1, 3, 21	8±12	0-100	20
BC	<0.01	0-22	2, 5, 9	6±3	0-30	5
Total	0.24					
1 Oct. 2011		Xu (%)				
u	AOT	min - max	P_{10},P_{50},P_{90}	mean	range	step
SU	0.06±0.08	1-95	15, 37, 60	37±17	0-100	20
DU	0.05±0.10	0-96	3, 16, 61	24±23	0-100	20
OC	0.05±0.09	1-95	5, 20, 55	25±18	0-100	20
SS	0.01±0.02	0-89	1, 3, 16	7±9	0-100	20
BC	0.01±0.02	0-25	3, 7, 12	7±4	0-30	5
Total	0.18					

Table 4 : Statistics about AOT's of each aerosol component from MERRA-2 analysis of 4 days in 2011

Each mixing ratio X_u cover the 0-100% range except BC which remains smaller than 25% on the four dates. The SU, DU, OC and SS X_u are defined between 0 and 100% with steps of 20%, and the BC X_u is defined between 0 and 30% with a step of 5%.

From the 5x5x5x5x6=3750 possible combinations, 148 combinations of the component X_u effectively occur on the 44 688 pixels of 2011/07/01. These 148 combinations of the components X_u define 148 aerosol models. (See Figure 7)

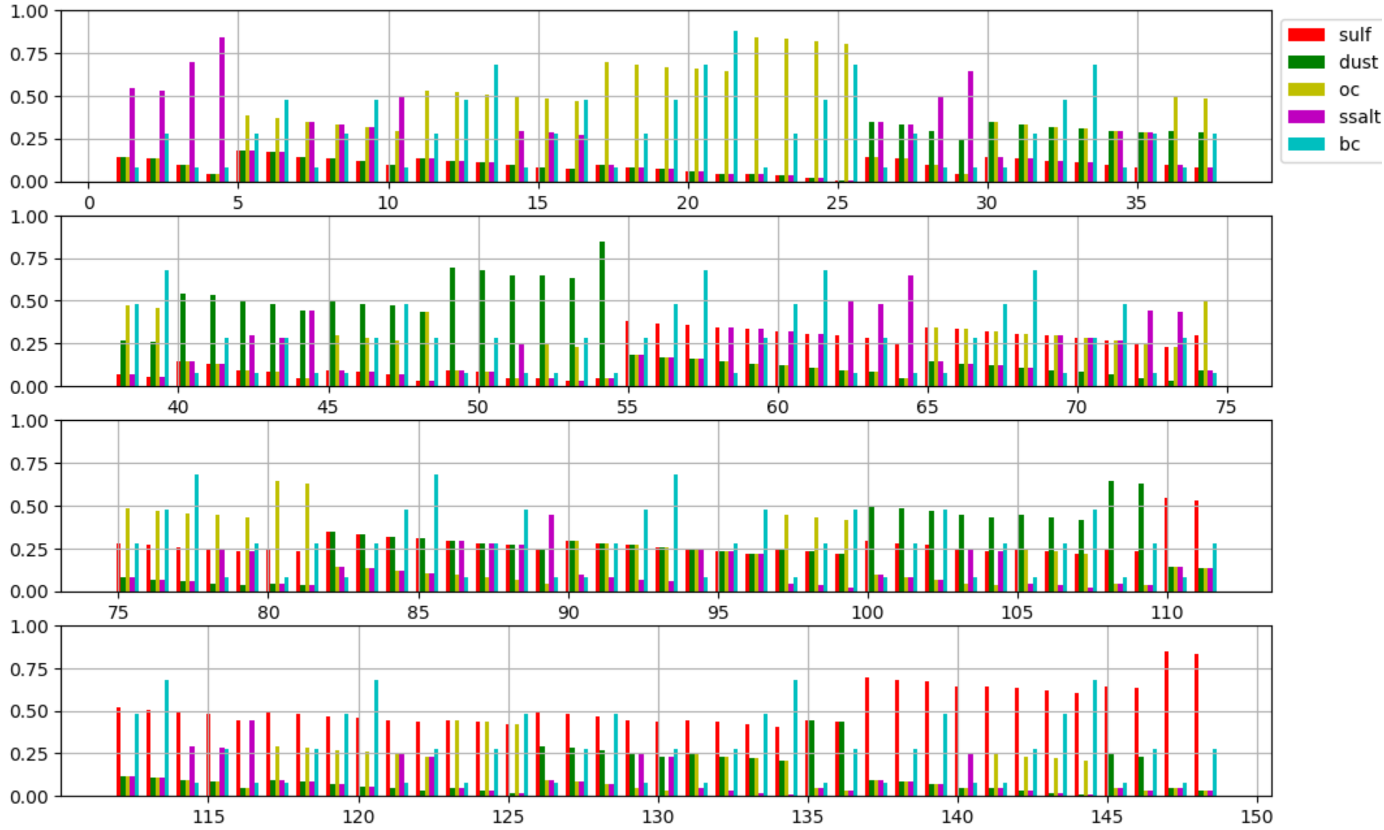

Figure 7: AOT's ratio's X_u of the 5 MERRA-2/CAMS aerosol components of the 148 aerosol model used in this study

4.2.2 Aerosol optical properties

In order to calculate easily the optical properties of these mixing, we directly associate one OPAC aerosol model/component to each component u from MERRA-2 or CAMS (see Table 5). For the moment the relative humidity is considered fixed to 80%

Table 5: Mapping between MERRA-2/CAMS aerosol component and OPAC for the computation of optical properties

MERRA-2/CAMS aerosol component	*OPAC model or component (RH=80%)*
SU/SU	Antarctic model
DU/DU	Desert model

OC/OM	Water soluble (waso) component
SS/SS	Maritime clean model
BC/BC	Soot component

The aerosol optical properties necessary for SMAC are then computed like this:

Spectral dependence of the AOT K (λ)=$^{\tau(\lambda)}/_{\tau}\,(550)$:

$$K(\lambda) = \sum_u K_u(\lambda) X_u$$

Single scattering albedo:

$$\varpi_0(\lambda) = \sum_u \varpi_0^u(\lambda) X_u$$

Phase function:

$$P(\theta, \lambda) = \sum_u P_u(\theta, \lambda) X_u$$

And the derived asymmetry parameter:

$$g(\lambda) = \frac{1}{2}\int_{-1}^{1} \mu P(\mu, \lambda)\, d\mu \text{ with } \mu = \cos(\theta)$$

These aerosol optical properties are plotted in Figure 8 and Figure 9.

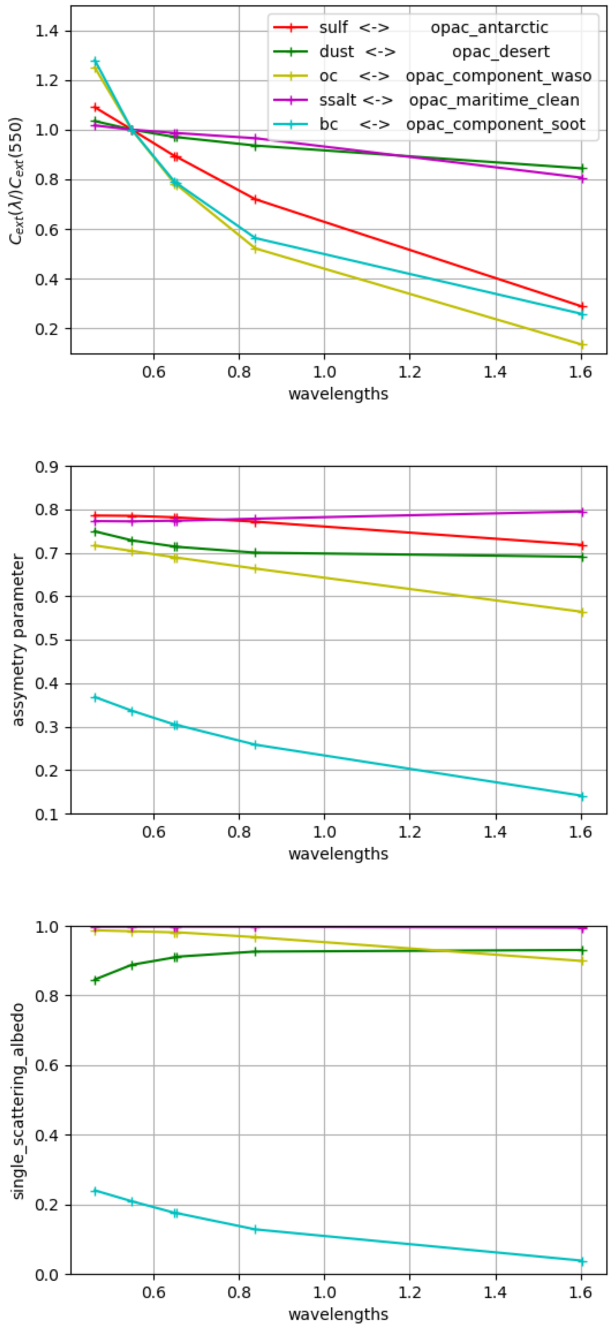

Figure 8: OPAC Aerosols components optical properties with RH=80% at the Proba-V spectral bands

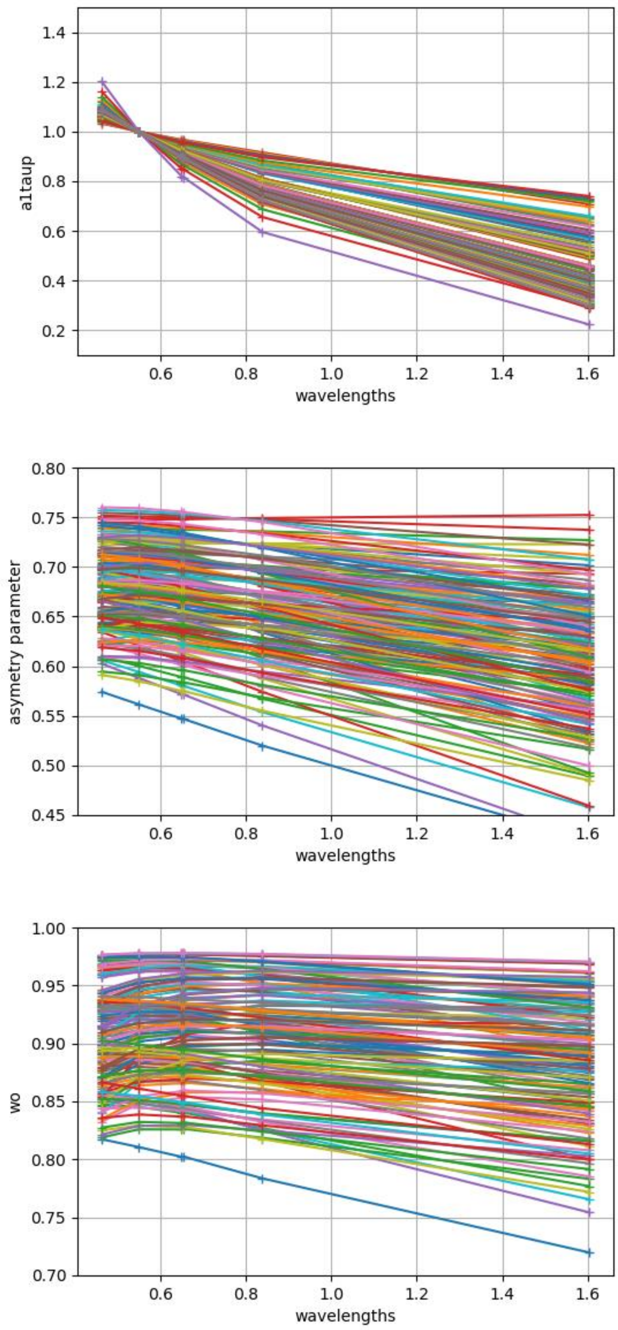

Figure 9 : 148 Aerosols mixtures optical properties at the Proba-V spectral bands.

4.3 Appendix 3: Computation of the SMAC coefficients

4.3.1 Processing chain

In Figure 10 is shown how SMAC coefficients are derived from basic data.

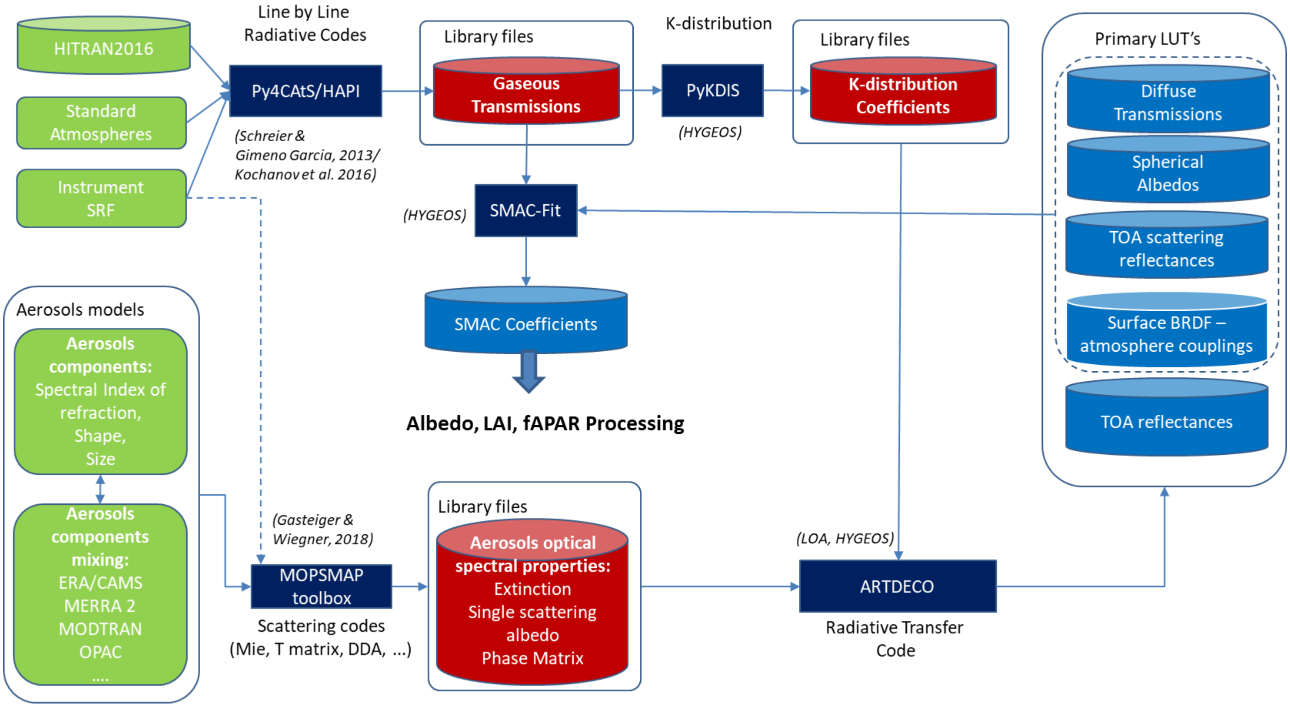

Figure 10 Organization of the radiative transfer tools at HYGEOS for computing atmospheric Look Up Tables from primary data

4.3.2 Gaseous absorption

With the RSRF 's data as described in the previous section, we computed the typical absorption based on the spectroscopic HITRAN 2012/2016 database (Gordon et al., 2017) and the line by line radiative transfer tools Py4Cats (Schreier et al., 2013) and/or HAPI (Kochanov et al., 2016). Then regression of gaseous transmission versus gas concentrations, air masses and barometric pressure (see Figure 11) were computed in order to yield SMAC coefficients fitting the gaseous absorption. Correlated K-distribution coefficients computed with the new tool PyKdis, developed by HYGEOS, are also obtained in this step, for further use in the simulation of real TOA radiances for both sensors.

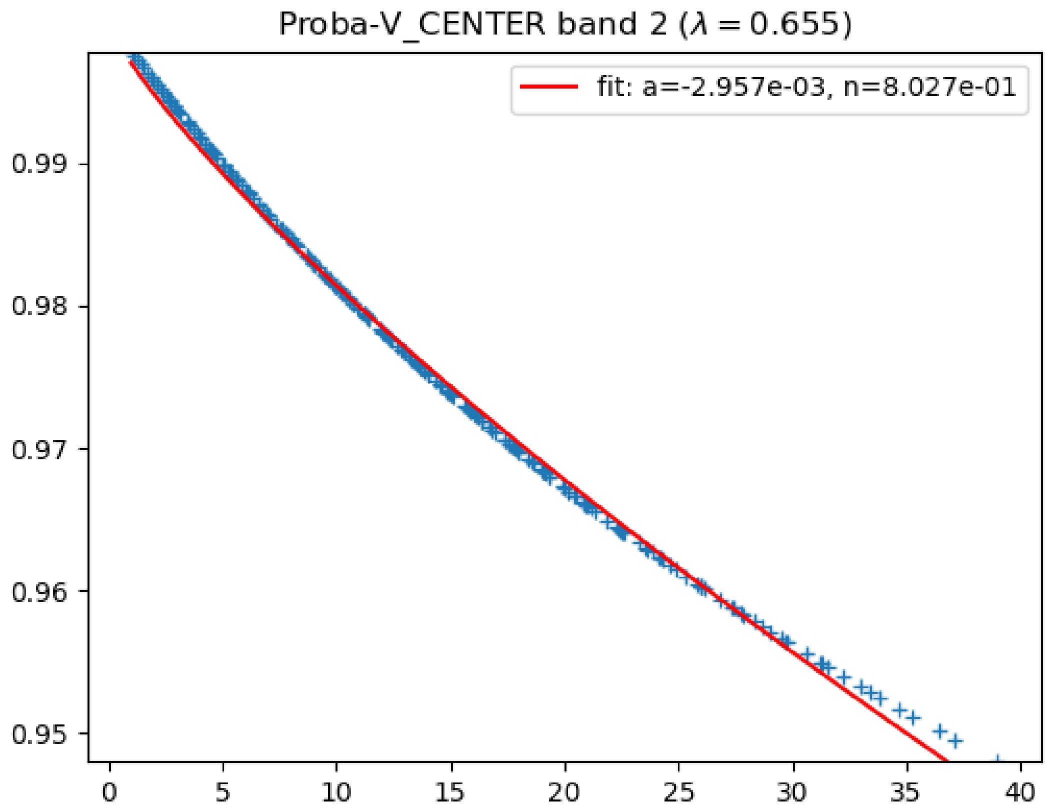

Figure 11: Example of the fit of water vapor transmission in band 2 of Proba-V Center camera. SMAC fitting model is T = exp (a . (m. U_{H2O})^n), where m is the air mass and U_{H2O} is the water vapor column

4.3.3 Radiative transfer computations

Radiative transfer equation for each pixel (geometry, band, AOT, Psurf) is solved independently using ARTDECO RT package (http://www.icare.univ-lille1.fr/projects/artdeco). The TOA reflectance computations are done for a black surface and no gaseous absorption in order to simulate scattering quantities used in 6S/SMAC, i.e.:

- TOA reflectance (ρ^{toa}) for aerosols and Rayleigh mixing, Aerosols and Rayleigh only
- Total (direct + diffuse) Transmission
- Spherical albedo

For each band, those optical quantities are simulated for various geometries, surface pressure, aerosol optical thicknesses… For example for the TOA reflectance:

- RAA: 121 values from 0 to 180°
- SZA : 38 values from 0 to 89° (but used only if <70°)
- VZA: 47 values from 0 to 89° (but used only if <70°)
- Surface pressure: 6 values from 600 to 1050 hPa
- AOT at 550 nm: 16 values from 0.01 to 1.5 (but used only if < 0.8)

Several multi-dimensional fits are performed to give the SMAC model parameters of scattering quantities. An estimation of the quality of the fit is also obtained, giving the potential to estimate the radiative transfer modeling error (see Figure 12).

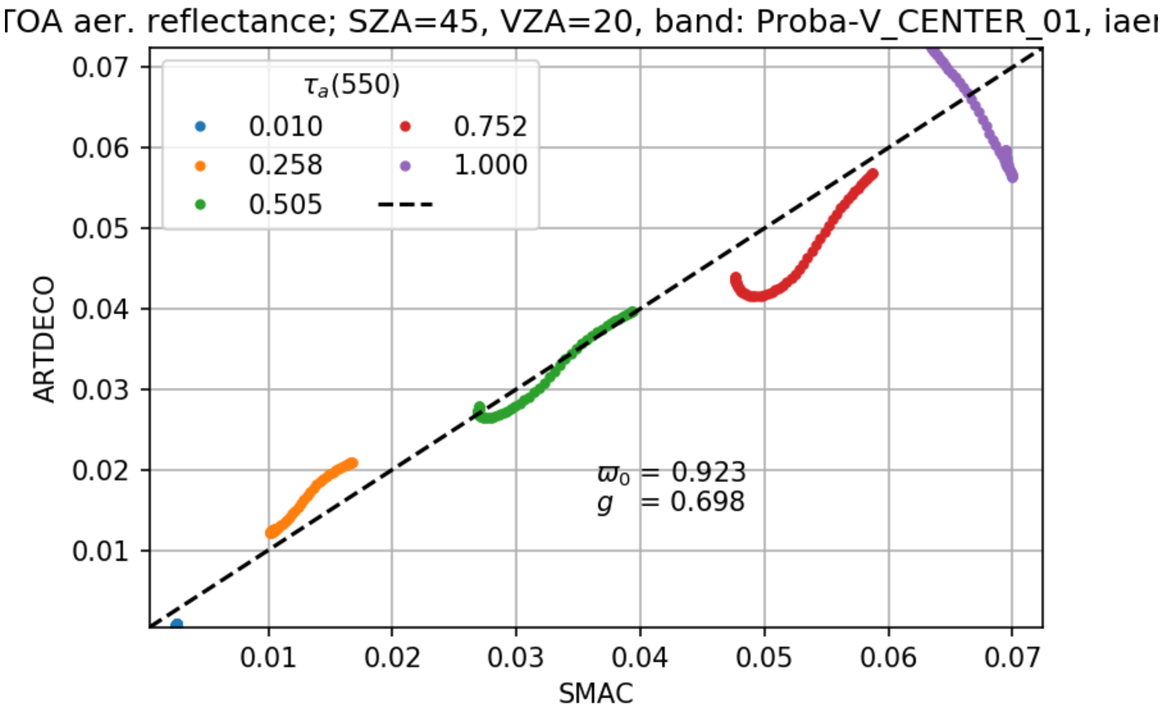

Figure 12: Example of accuracy of the SMAC model compared to ARTDECO. Aerosol TOA reflectance for band 01 of Proba-V center camera for one particular SZA and VZA and for all azimuth, for AOT at 550 nm ranging from 0.01 to 1 and for the aerosol model #1. The fit was performed for all VZA < 60, SZA <70, AOT (550) <0.76, all azimuths. The accuracy decreases above an AOT at 550 nm of ~ 0.5

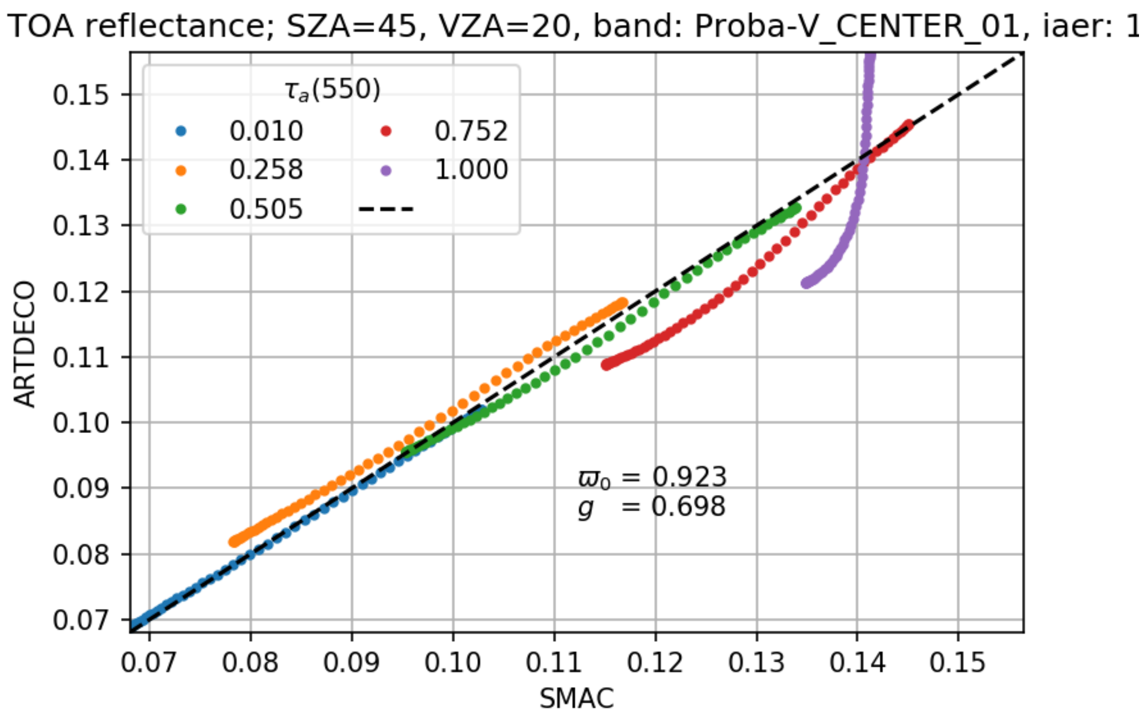

Figure 13 : Same as Figure 12 but for TOA atmospheric reflectance.

F. Schreier and S. Gimeno Garcia (2013). Py4CAtS – Python Tools for Line-by-Line Modelling of Atmospheric Radiative Transfer. *In Robert F. Cahalan and Jürgen Fischer (editors), Radiation Processes in the Atmosphere and Ocean (IRS 2012): Proceedings of the International Radiation Symposium (IRC/IAMAS) Volume 1531 of AIP Conference Proceedings*, pages **123 - 126**. American Institute of Physics, 2013. doi: 10.1063/1.4804723 https://atmos.eoc.dlr.de/tools/Py4CAtS

I. E. Gordon, L. S. Rothman, C. Hill, R. V. Kochanov, Y. Tan, *et al.*, (2017) The HITRAN2016 molecular spectroscopic database, *J. Quant. Spectrosc. Radiat. Transfer* **203**, 3-69 (2017)

R.V. Kochanov, I.E. Gordon, L.S. Rothman, P. Wcislo, C. Hill, J.S. Wilzewski (2016). HITRAN Application Programming Interface (HAPI): A comprehensive approach to working with spectroscopic data, *J. Quant. Spectrosc. Radiat. Transfer,* **177**, 15-30 (2016). https://hitran.org/hapi

Hess, M.; Koepke, P. & Schult, I, (1998). Optical Properties of Aerosols and Clouds: The Software Package OPAC. *Bulletin of the American Meteorological Society*, 1998, **79**, 831-844

4.4 Appendix 4: Implementation of atmospheric correction

Flowchart

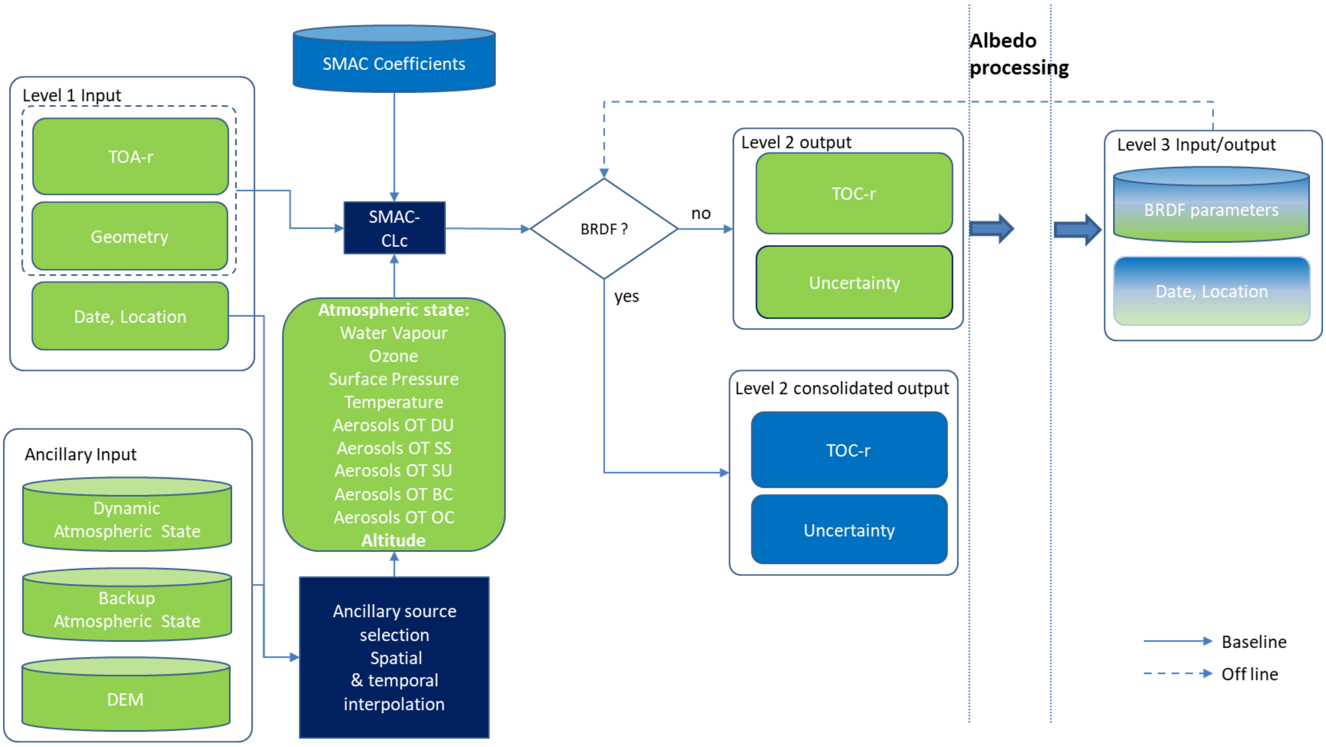

Input reading

The elevation map and its uncertainty (`elev` and `Delev`) are read from the DEM auxiliary file <u>once</u> (even for multiple file processing).

The image inputs are read from Level 1 files (section 1). For each pixel of the image, the following quantities are read:

- The TOA radiance for each sensor channel λ: `TOA-r`(λ)
- The corresponding error: `DTOA-r`(λ),
- The corresponding solar extra-terrestrial irradiance `Es`(λ)
- The sun zenith angle (`SZA`), the sun azimuth angle (`SAA`), the view zenith angles (`VZA, VZA_SWIR`), and the viewing azimuth angle (`VAA, VAA_SWIR`),
- The latitude and longitude: `lat, lon`,

The <u>name of the sensor, date and mean time of acquisition (in UTC)</u> should be written in the file as an <u>attribute</u>. Indeed, the name of the sensor and the date of acquisition allow reading the right SMAC coefficients `coeffs` while the date allows reading the daily MERRA-2/CAMS auxiliary files as described in Section 1.2.2.

Pixel masking

The cloud contaminated are masked and not further processed. The selection is based on the cloud flag already present in the `input file`. The idea is to keep the clearest pixels only. It is done by selecting pixels for which the flag is `0`. We mask out also pixels for which SZA is above 90°.

Spatial and temporal interpolation of auxiliary data

From `elev`, `Delev`, `lat`, `lon`, the pixel altitude **z** and its uncertainty **Δz** is obtained through a nearest neighbor interpolation.

The sea-level pressure **P₀**, the temperature above ground **T**, the total ozone column $\boldsymbol{U_{O_3}}$, the total column water vapor $\boldsymbol{U_{H_2O}}$ and the AOT at 550 nm $\boldsymbol{\tau_a^{550}}$, $\boldsymbol{\tau_{a;DU}^{550}}, \boldsymbol{\tau_{a;SU}^{550}}, \boldsymbol{\tau_{a;OC}^{550}}, \boldsymbol{\tau_{a;BC}^{550}}, \boldsymbol{\tau_{a;SS}^{550}}$ are obtained respectively from the `SLP/msl`, `T10M/t2m`, `TO3/gtco3`, `TQV/tcwv` and `TOTEXTTAU/aod550`, `DUEXTTAU/duaod550`, `SUEXTTAU/suaod550`, `OCEXTTAU/omaod550`, `BCEXTTAU/bcaod550`, `SSEXTTAU/ssaod550` MERRA-2/CAMS auxiliary data (see section 1.2.2) through a spatial and temporal linear interpolation

The auxiliary data are then converted from MERRA-2/CAMS to SMAC units:

1. Table: MERRA-2 and SMAC units

Variable	MERRA-2 unit	SMAC unit	Conversion factor
U_{O3}	Dobson	cm.atm	1e-3
U_{H2O}	$kg.m^{-2}$	$g.cm^{-2}$	1e-1
P_0	Pa	hPa	1e-2

2. Table: CAMS and SMAC units

Variable	MERRA-2 unit	SMAC unit	Conversion factor
U_{O3}	$kg.m^{-2}$	cm.atm	1e-3/2.1415e-2(= 46.7)
U_{H2O}	$kg.m^{-2}$	$g.cm^{-2}$	1e-1
P_0	Pa	hPa	1e-2

Then, the surface pressure $\mathbf{P_s}$ and its uncertainty $\mathbf{\Delta P_s}$ are computed using Eq. (22), (23), and (24), (25), (26).

Aerosol model selection

Select the aerosol model number (between 148 models), by minimizing the distance in a 5-dimensional space corresponding to the 5 AOT ratios $\{X_u,\ u \in \{\mathrm{DU, SU, OC, BC, SS}\}\}$ of the 5 aerosol components

$X_u = \boldsymbol{\tau_{a;u}^{550}} / \boldsymbol{\tau_a^{550}}$

iaero = $\mathrm{Min}\{\sum_u (\boldsymbol{X_u} - X_{u,i})^2\}_{i=0,147}$.

The $X_{u,i}$ basis for the 148 predefined models are stored in a text file and read once.

An example of inputs is given in Figure 14.

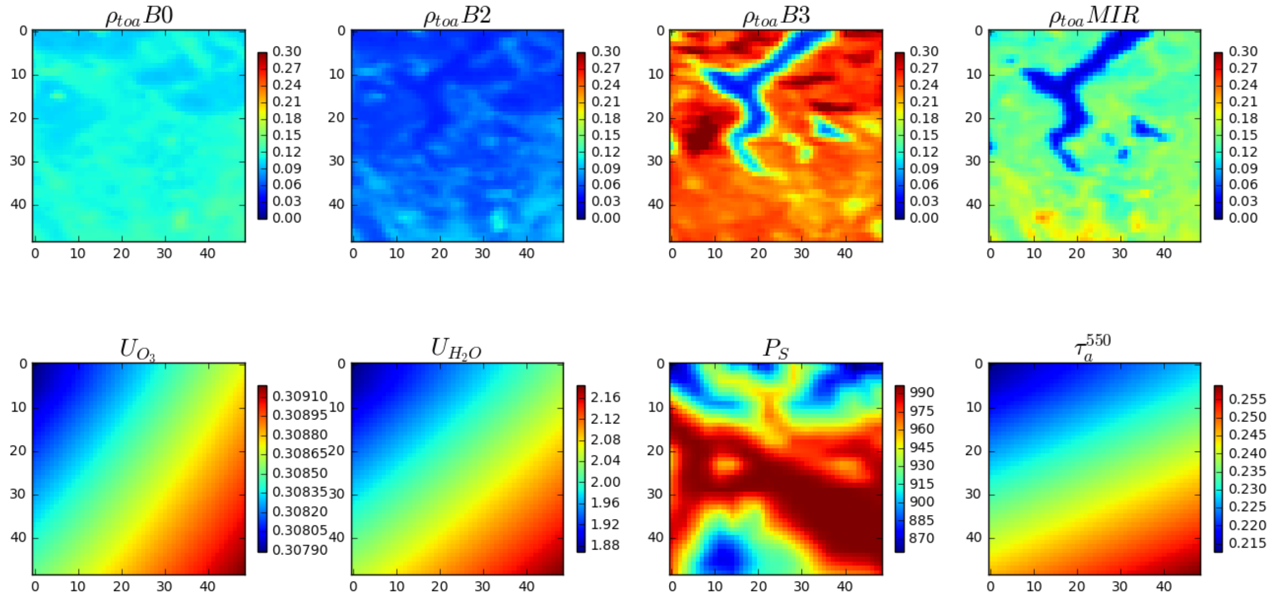

Figure 14: Example on VGT data. Extraction of a 49x49 pixel box around AERONET station of Ispra on 1st of June 1999. Input TOA reflectances for each VGT band and interpolated auxiliary data with SMAC units. White pixels are clouds.

SMAC-CL

A version of SMAC, called SMAC-CL, has been developed with the OPEN CL graphics card programming language that includes the error propagation model with a Python interface. It can also run on CPU

Preparation of arrays for GPU

The input arrays have to be reorganized in order to be processed by the graphic card with a maximum efficiency.
For example, here is shown the definition of the SMAC-CL routine within the Python interface:

```
def run(self, coeffs, tetas, tetav, phis, phiv, uh2o, uo3, taup550, pressure, rtoa, k1p, k2p, iaero XBLOCK=512, XGRID=512, NBLOOP=1):
Arguments:
        - coeffs:  an array containing SMAC coefficients, of length NBAND, of type type_coeff
        - tetas: SZA float32 arrays of dimension (XBLOCK, XGRID, Z) where Z is 3rd dimension of pixels
        - tetav: VZA float32 arrays of dimension (XBLOCK, XGRID, Z) where Z is 3rd dimension of pixels
        - phis: SAA float32 arrays of dimension (XBLOCK, XGRID, Z) where Z is 3rd dimension of pixels
        - phiv: VAA float32 arrays of dimension (XBLOCK, XGRID, Z) where Z is 3rd dimension of pixels
        - uh2o : Water vapour column float32 arrays of dimension (XBLOCK, XGRID, Z) where Z is 3rd dimension of pixels
        - uo3  : Ozone column float32 arrays of dimension (XBLOCK, XGRID, Z) where Z is 3rd dimension of pixels
```

- taup550: AOT at 550 nm float32 arrays of dimension (XBLOCK, XGRID, Z) where Z is 3rd dimension of pixels
- pressure: Surface pressure float32 arrays of dimension (XBLOCK, XGRID, Z) where Z is 3rd dimension of pixels
- rtoa : TOA reflectance float32 arrays of dimension (XBLOCK, XGRID, Z, NB) where Z is 3rd dimension of pixels, and NB is the number of bands
- k1p : k1/k0 coefficient ratio of the first RossThick Li-Sparse kernel, float32 arrays of dimension (XBLOCK,XGRID,Z, NB) where Z is 3rd dimension of pixels, and NB is the number of bands It is by default 0 for a lambertian surface.
- k2p : k2/k0 coefficient ratio of the second RossThick Li-Sparse kernel, float32 arrays of dimension (XBLOCK,XGRID,Z, NB) where Z is 3rd dimension of pixels, and NB is the number of bands It is by default 0 for a lambertian surface.
- iaero: aerosol model index (between 0 and 147) int array of dimension (XBLOCK, XGRID, Z) where Z is 3rd dimension of pixels
- XBLOCK and XGRID: control the number of blocks and grid size for the GPU execution
- NBLOOP: number of runs within a thread for the same pixel (should be used for Monte Carlo draws)

The SMAC-CL procedure inputs correspond to the following quantities described in this document: `coeffs, SZA, VZA, SAA, VAA,` $\boldsymbol{U_{\mathrm{H_2O}}}, \boldsymbol{U_{\mathrm{O_3}}}, \boldsymbol{\tau_a^{550}}$, $\mathbf{P_s}$, `TOA-r(`λ`), k1p, k2p, iaero`.
The run method is called twice, one for the VIS-NIR bands and one for the SWIR band.
For the moment k1p and k2p arrays are set to zero, that means that the surface is considered lambertian.
All the image inputs are multidimensional. The angles and auxiliary data are 3-dimensional, with the dimensions `XBLOCK, XGRID` being adapted to the graphic card. The default values of 512 for both parameters is good starting choice but could be further optimized. The 3rd dimension Z is up to the user and is the number of pixels each GPU thread will process. The input TOA reflectance array has a 4th dimension which is the number of bands to be corrected. The keyword `NBLOOP` stands for the number of different runs for each pixel. For the moment, it is set to 1.
An idea of SMAC-CL computation time is: 12 s on a commercial PC equipped with a GTX 600 NVidia graphic card for a 512x512 image, 15 bands, and 1000 Monte Carlo runs for each pixel.

The outputs of the SMAC-CL routine are:

- The AC corrected directional reflectance $\mathbf{R}_{toc}$ for each sensor channel λ
- The Jacobians $\boldsymbol{J}_{\mathbf{R}_{toc}}^{R_{toa}}, \boldsymbol{J}_{\mathbf{R}_{toc}}^{U_{O_3}}, \boldsymbol{J}_{\mathbf{R}_{toc}}^{U_{H_2O}}, \boldsymbol{J}_{\mathbf{R}_{toc}}^{U_{P_S}}, \boldsymbol{J}_{\mathbf{R}_{toc}}^{\tau_a^{550}}$

An example of the Jacobians is given in Figure 15.

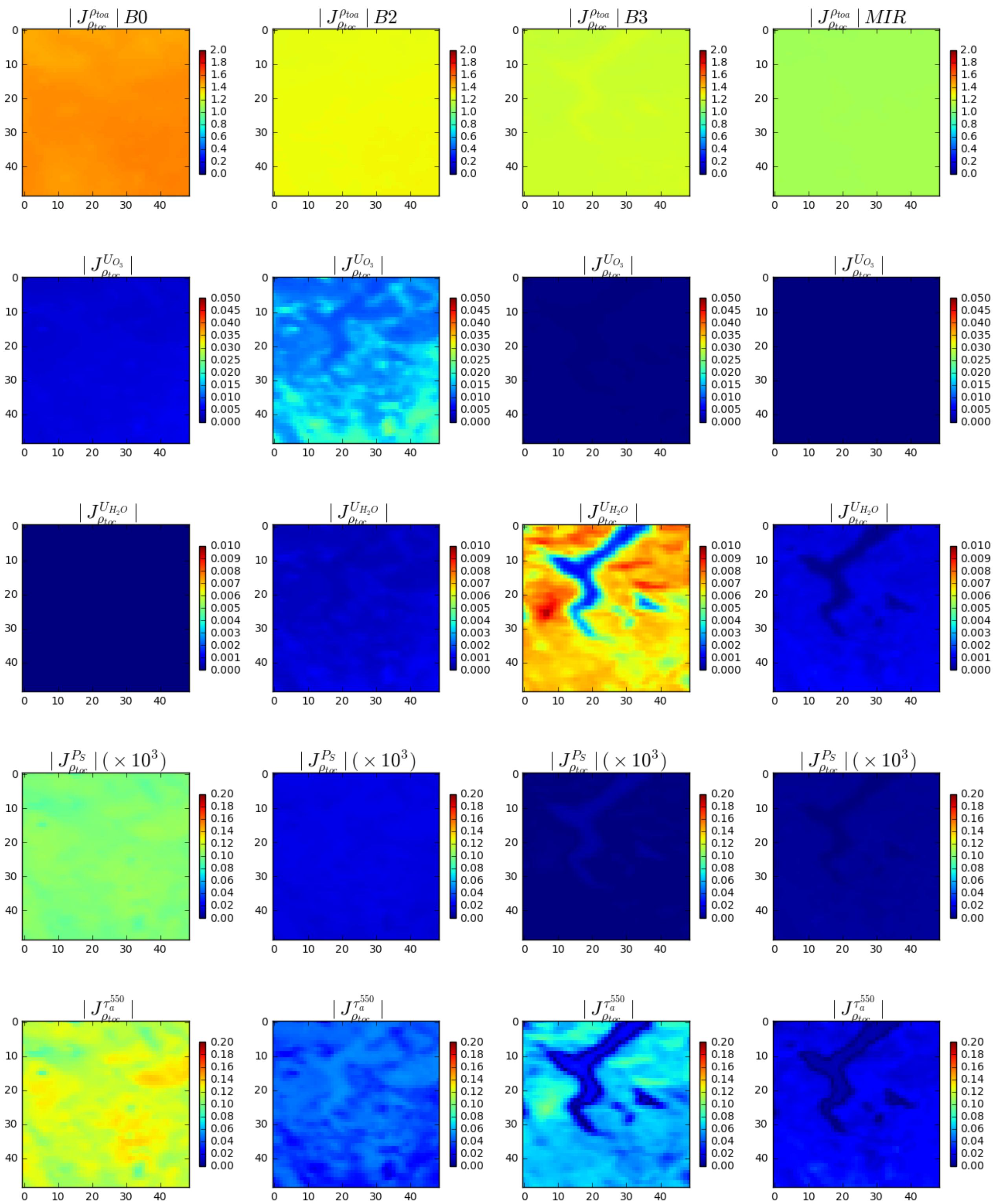

Figure 15: Same as Figure 14 but for the absolute values of the output Jacobians; in SMAC units.

Outputs

The outputs of AC module are:

- The AC corrected directional reflectance $\mathbf{R}_{toc}$ for each sensor channel λ,
- The associated uncertainties $\Delta\mathbf{R}_{toc}$ for each sensor channel λ,

TOC directional reflectances and Jacobians are direct outputs of the SMAC procedure (done in the GPU) while the associated uncertainties are post-processed in the CPU as described in section 2.2.3., Eq. (20). The quantities used are:

- The Jacobians $\boldsymbol{J}_{\mathbf{R}_{toc}}^{R_{toa}}, \boldsymbol{J}_{\mathbf{R}_{toc}}^{U_{O_3}}, \boldsymbol{J}_{\mathbf{R}_{toc}}^{U_{H_2O}}, \boldsymbol{J}_{\mathbf{R}_{toc}}^{U_{P_S}}, \boldsymbol{J}_{\mathbf{R}_{toc}}^{\tau_a^{550}}$
- `DTOA-r(`λ`)`, $\Delta\boldsymbol{U}_{\boldsymbol{O_3}}$, $\Delta\boldsymbol{U}_{\boldsymbol{H_2O}}$, $\Delta\boldsymbol{P}_{\boldsymbol{S}}$, $\Delta\boldsymbol{\tau}_{\boldsymbol{a}}^{\mathbf{550}}$ (see Table 2)

The projection and the attributes of the input TOA reflectances are kept. Nevertheless, the longitude and latitude fields are also written in the output file for simplicity.
An example of the outputs is given in Figure 16.

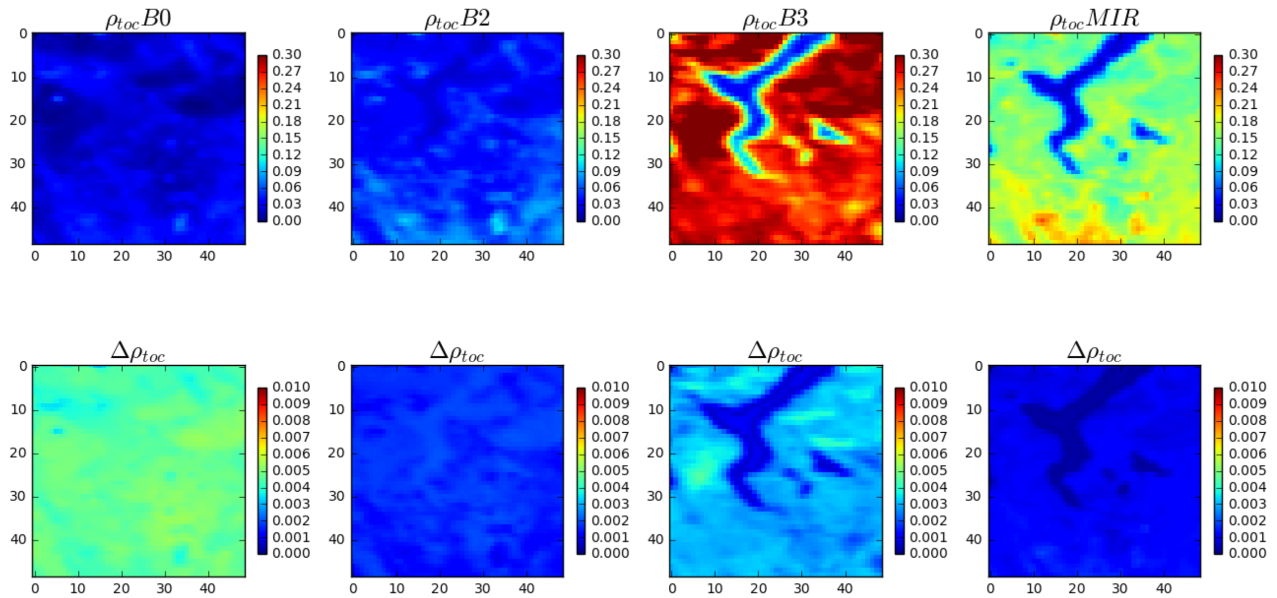

Figure 16: Same as Figure 14 but for output TOC spectral reflectances and their respective errors.